OPEN ACCESS Freely available online

PLoS GENETICS

Roles of the Espin Actin-Bundling Proteins in the Morphogenesis and Stabilization of Hair Cell Stereocilia Revealed in CBA/CaJ Congenic Jerker Mice

Gabriella Sekerková[1], Claus-Peter Richter[2,3], James R. Bartles[1,3]*

1 Department of Cell and Molecular Biology, Northwestern University Feinberg School of Medicine, Chicago, Illinois, United States of America, **2** Department of Otolaryngology, Northwestern University Feinberg School of Medicine, Chicago, Illinois, United States of America, **3** Hugh Knowles Center for Clinical and Basic Science in Hearing and Its Disorders, Northwestern University Feinberg School of Medicine, Chicago, Illinois, United States of America

Abstract

Hearing and vestibular function depend on mechanosensory staircase collections of hair cell stereocilia, which are produced from microvillus-like precursors as their parallel actin bundle scaffolds increase in diameter and elongate or shorten. Hair cell stereocilia contain multiple classes of actin-bundling protein, but little is known about what each class contributes. To investigate the roles of the espin class of actin-bundling protein, we used a genetic approach that benefited from a judicious selection of mouse background strain and an examination of the effects of heterozygosity. A congenic jerker mouse line was prepared by repeated backcrossing into the inbred CBA/CaJ strain, which is known for excellent hearing and minimal age-related hearing loss. We compared stereocilia in wild-type CBA/CaJ mice, jerker homozygotes that lack espin proteins owing to a frameshift mutation in the espin gene, and jerker heterozygotes that contain reduced espin levels. The lack of espins radically impaired stereociliary morphogenesis, resulting in stereocilia that were abnormally thin and short, with reduced differential elongation to form a staircase. Mean stereociliary diameter did not increase beyond ~0.10–0.14 μm, making stereocilia ~30%–60% thinner than wild type and suggesting that they contained ~50%–85% fewer actin filaments. These characteristics indicate a requirement for espins in the appositional growth and differential elongation of the stereociliary parallel actin bundle and fit the known biological activities of espins in vitro and in transfected cells. The stereocilia of jerker heterozygotes showed a transient proximal-distal tapering suggestive of haploinsufficiency and a slowing of morphogenesis that revealed previously unrecognized assembly steps and intermediates. The lack of espins also led to a region-dependent degeneration of stereocilia involving shortening and collapse. We conclude that the espin actin-bundling proteins are required for the assembly and stabilization of the stereociliary parallel actin bundle.

Citation: Sekerková G, Richter C-P, Bartles JR (2011) Roles of the Espin Actin-Bundling Proteins in the Morphogenesis and Stabilization of Hair Cell Stereocilia Revealed in CBA/CaJ Congenic Jerker Mice. PLoS Genet 7(3): e1002032. doi:10.1371/journal.pgen.1002032

Editor: Wayne N. Frankel, The Jackson Laboratory, United States of America

Received October 26, 2010; **Accepted** February 2, 2011; **Published** March 24, 2011

Funding: This work was supported by NIH grant R01 DC004314 to JRB and NSF grants IBN-077476 and IBN-0415901 to C-PR. The scanning electron microscopy was performed in the EPIC facility of the NUANCE Center at Northwestern University, which is supported by the NSF-NSEC, NSF-MRSEC, the Keck Foundation, the State of Illinois, and Northwestern University. The funders had no role in study design, data collection and analysis, decision to publish, or preparation of the manuscript.

Competing Interests: The authors have declared that no competing interests exist.

* E-mail: j-bartles@northwestern.edu

Introduction

A stunning example of cytoskeleton-mediated morphogenesis is the formation of hair cell stereocilia, which act as primary mechanosensory detectors in the auditory and vestibular systems [1,2]. Stereocilia are fingerlike projections that contain a specialized cytoskeletal element, the parallel actin bundle [3], aligned axially at their core. The parallel actin bundle, which consists of hexagonally packed unidirectional actin filaments cross-linked by actin-bundling proteins to produce a regular ~12–13 nm (center-to-center) interfilament spacing, exhibits the properties of a molecular scaffold that sets the dimensions of stereocilia and influences their mechanical properties [3–5]. During development, highly precise staircase collections of stereocilia are produced from microvillus-like precursors as their parallel actin bundle scaffolds selectively undergo an increase in diameter, through the addition of more actin filaments to the parallel actin bundle, and their constituent actin filaments elongate or shorten [4,5]. The plasma membrane of the stereocilium remains in close proximity to the parallel actin bundle throughout morphogenesis, so that increases in stereociliary diameter reflect increases in the number of actin filaments in the parallel actin bundle and changes in stereociliary length correspond to changes in the length of the actin filaments in the parallel actin bundle [6]. The dimensions of stereocilia vary in a remarkably regular way, not only within a given collection, but also according to hair cell type and position in the cochlea or vestibular system [7–10]. This attests to an impressive degree of spatial precision in actin-cytoskeletal regulation. A growing list of deaf mutant mice with malformed stereocilia demonstrates the importance of stereociliary morphogenesis to hair cell mechanoelectrical signal transduction [11,12].

The modifications in parallel actin bundle dimensions that underlie stereociliary morphogenesis are presently thought to involve actin-bundling proteins [13–17], actin-capping proteins [18–20], unconventional myosin motors and their cargoes

Author Summary

Stereocilia are the fingerlike projections of inner ear hair cells that detect sound and motion. Stereocilia grow to specific lengths and diameters and form staircase-like arrays. The changes in size appear to be driven by matching alterations in the dimensions of an underlying molecular scaffold consisting of a bundle of actin filaments cross-linked by actin-bundling proteins. To elucidate the roles of the espin actin-bundling proteins in hair cell stereocilia, we carry out an in-depth accounting of stereociliary size and shape in the jerker mutant mouse, which lacks the espin proteins because of a mutation in the espin gene. We examine a new and improved jerker mouse with a genetic background known for high-quality lifelong hearing. We find that, in the absence of espins, stereocilia do not increase in diameter or complete their elongation, but instead bend, shorten, and disappear. Although the specifics vary according to inner ear region, the stereociliary defects are profound and can readily account for the deafness and balance problems of jerker mice and humans with certain espin gene mutations. Even reducing espin levels by one-half leads to temporary defects in stereociliary diameter. Thus, espins play crucial roles in the formation and maintenance of hair cell stereocilia.

[21–23]. Although multiple classes of actin-bundling protein have been identified in hair cell stereocilia, relatively little is known about what each class contributes [13–17]. One class of actin-bundling protein implicated in hair cell stereocilia is the espin family [24]. Discovered originally in Sertoli cell junctional plaques [25], espins are encoded by a single gene, but are produced in multiple isoforms [24–27]. Espins bind to and cross-link actin filaments into parallel actin bundles in vitro with high affinity and in a Ca^{2+}-insensitive manner [28–30], exert a potent cooperative effect on the twist of actin filaments in parallel actin bundles [31] and elicit a dramatic, concentration-dependent elongation of parallel actin bundles in cells [27,32–34]. In hair cell stereocilia, espin antibody staining is detected along the length of the parallel actin bundle in the body of the stereocilium, both in adulthood and during morphogenesis, but not in the rootlet [14,16,32,35,36]. Espin expression and accumulation in stereocilia are hallmarks of hair cell differentiation in situ and by stem cells in culture [35,37,38]. In addition, the espin gene is the target of mutations associated with deafness and vestibular dysfunction, including the jerker mutation in mice [14,39,40].

The jerker mutation is a spontaneous mutation noted in the collection of a mouse fancier and first described in 1941 [41–43]. Homozygous jerker mice exhibit the stereotyped shaker-waltzer behavior indicative of hair cell defects, including deafness, circling, head tossing and hyperactivity. In 2000, the jerker mutation was shown to be a frameshift mutation in the espin gene (c.2426delG; *Espn*^{je}) on mouse chromosome 4 [14], and this was verified by independent physical mapping studies [44]. Because homozygous jerker mice lack espin proteins and jerker heterozygotes contain approximately half-normal espin levels [14], the examination of jerker mice promises to reveal a great deal about the functions of espins. Earlier studies examining stereociliary ultrastructure in inbred jerker mice with uncharacterized genetic backgrounds detected the degeneration of stereocilia and loss of hair cells in jerker homozygotes [33,45–47]. Although the results were encouraging, these earlier studies did not compare wild-type mice of the same genetic background and either were not systematic or examined only a single hair cell type and inner ear location. In addition, the effects on the vestibular system [45] were not investigated in detail. Importantly, the detection of a related group of degenerative changes in jerker heterozygotes with later onset [45–48] was difficult to reconcile with the presumed recessive nature of the jerker mutation. This naturally raised concerns about possible complications owing to strain-specific genetic modifier effects or age-related hearing loss, which have been detected in a number of mouse strains [49]. A recent proteomic analysis of stereocilia detected espins at lower levels than some other actin-bundling proteins [17], raising additional questions about the roles of espins.

To help elucidate the roles of espins in hair cell stereocilia, we have carried out a systematic scanning electron microscopic study of hair cell stereocilia examining a congenic jerker mouse line we prepared using the CBA/CaJ inbred strain. The CBA/CaJ strain was chosen for the genetic background because CBA/CaJ mice exhibit excellent hearing and minimal age-related hearing loss [50]. Unlike earlier studies, we compared jerker homozygotes and heterozygotes to wild-type mice of the same genetic background, analyzed hair cells from multiple inner ear locations in the cochlea and vestibular system, examined specimens without metal coating, measured stereociliary width and length and focused on the critical period of early postnatal development. We determined that the absence of espin proteins drastically alters stereociliary morphogenesis, resulting in marked decreases in stereocilium diameter, length and stability. In addition, we uncovered an informative group of transient developmental defects in jerker heterozygotes, which contain reduced espin levels.

Results

We generated a congenic jerker mouse line (CBA/CaJ.JE/LeJ-*Espn*^{je}) by repeated backcrossing for 13–15 generations into the CBA/CaJ inbred strain. Because of their excellent hearing and minimal age-related hearing loss, CBA/CaJ mice are often preferred for research on hearing [49,50]. This step was taken out of a concern that genetic modifier effects or age-related hearing loss, which have been detected in many mouse strains [49], might account for some of the inner ear defects noted previously by others in inbred jerker mice with uncharacterized genetic backgrounds. In addition, we identified multiple defects in mice of the standard inbred jerker mouse strain available commercially from the Jackson Laboratory (JE/LeJ), including simplified cerebellar lobulation (Figure S1A-S1D) and smaller, misshapen eyeballs, featuring a constricted pupil and a cloudy and often-deformed lens (Figure S1E and S1F). The cerebellum and eye both contain espins in wild-type mice [26,27]. The cerebellum and eye defects were not observed in CBA/CaJ mice or in the newly prepared congenic jerker mouse line with the CBA/CaJ genetic background (Figure S1A-S1F). Although largely uncharacterized, JE/LeJ mice are known to be homozygous for the nonagouti (*a*), ruby-eye (*Hps6*^{ru}) and flexed-tail (*f*) mutations. For brevity, CBA/CaJ.JE/LeJ-*Espn*^{je}/*Espn*^{je}, CBA/CaJ.JE/LeJ-+/*Espn*^{je} and CBA/CaJ mice will hereafter be referred to as *je/je*, +/*je* and +/+ mice, respectively.

+/+, +/*je* and *je/je* mice did not differ in outward appearance, except that *je/je* mice exhibited circling, head tossing and hyperactivity. In contrast, +/*je* mice did not display these behaviors and appeared indistinguishable from +/+ mice. In these respects, mice of the new congenic jerker mouse line resembled their JE/LeJ counterparts. When compared at low magnification using the dissection microscope and the scanning electron microscope, we noted no obvious differences in inner ear anatomy between +/+, +/*je* and *je/je* mice. Sequence analysis of

PCR products obtained from genomic DNA and of espin cDNAs confirmed the presence of the c.2426delG espin gene mutation [14] in *je/je* mice and +/*je* mice. Western blot analysis using a well-characterized affinity purified rabbit polyclonal antibody [51] that reacts with all known espin isoforms, including epitopes upstream of the frameshift mutation [27], confirmed the absence of espin proteins in *je/je* mice and the presence of reduced espin protein levels in +/*je* mice. Figure 1A illustrates these results for homogenates of testis and kidney, the two relatively large espin-expressing organs we routinely analyze on western blots [14] that are rich sources of the largest and smallest espin isoforms, espin 1 (~105–110 kDa) and espin 4 (~22–28 kDa), respectively [27]. Immunolabeling of inner ear specimens with this same espin antibody revealed intense staining of hair cell stereocilia in +/+ and +/*je* mice (Figure 1B–1F) and confirmed the absence of espin proteins in the hair cells and stereocilia of *je/je* mice (Figure 1G–1I). Figure 1D–1I illustrates these results for the stereocilia of vestibular hair cells in the extrastriolar region of the utricular macula, which were labeled with espin antibody in +/*je* mice (Figure 1E), but not in *je/je* mice (Figure 1H).

To definitively establish the effects of the jerker mutation and the resultant deficiency of espin proteins on hair cell stereocilia, we used the high-resolution imaging technique of scanning electron microscopy to carry out a systematic analysis of stereocilia in the cochlea and vestibular system of +/+, +/*je* and *je/je* mice. First, we provide a qualitative assessment of the stereocilia, and then we present measurements of their width and length as a means to gauge changes in the dimensions of the stereociliary parallel actin bundle scaffold.

Overview

Cochlea. The cochlear hair cells of *je/je* mice exhibited dramatic stereociliary defects. This was the case for inner and outer hair cells and in all regions along the cochlea. In general, stereocilia were thinner and shorter than in +/+ mice and showed progressive degeneration, involving bending, shortening and loss. Despite the severity of these defects, the fingerlike projections emanating from the apical surface of cochlear hair cells in *je/je* mice looked relatively similar to those in +/+ mice at the earliest stage of differentiation examined, on the day of birth or postnatal day 0 (P0) (Figure 2A, 2G, 2M and 2S). The main difference was that the projections observed in *je/je* mice appeared somewhat thinner than those in +/+ mice (Figure 2A, 2G, 2M and 2S). At early stages, the customary one row of inner hair cells and three rows of outer hair cells were easy to recognize in *je/je* mice (Figure S2A), and the numbers of their surface projections were similar to those in +/+ controls (Figure 2A–2D, 2G–2J, 2M–2P and 2S–2V; and see P5 data in Table 1). We also detected a graded elongation of stereociliary precursors to form a rudimentary staircase at the correct (kinociliary) pole of the cell (Figure 2A–2C, 2G–2I, 2M–2O and 2S–2U), which showed the usual preferential alignment toward the abneural edge of the epithelium (Figure S2A).

In +/+ mice, the morphogenesis of stereocilia beyond P0 involved increases in diameter and adjustments in length to produce more mature staircases consisting of ~3 rows of stereocilia (Figure 2A–2F and 2M–2R and Figure 3A). While tall stereociliary precursors in the apical region of the cochlea showed a small amount of additional elongation (Figure 2A, 2E, 2M and 2Q), those on outer hair cells in the middle and basal regions actually became shorter (Figure 2B and 2F; see more below). In addition, the collection of stereociliary precursors on outer hair cells was modified to produce three clearly discernible rows with the characteristic "W" shape (Figure 2C–2F), which required the efficient clearance of projections from other regions of the apical surface. As hair cell differentiation proceeded, differences between the stereocilia of *je/je* and +/+ mice became more pronounced. For example, differences from +/+ controls were already more obvious in the base of the cochlea than in the apex at P0 (Figure 2A–2C, 2G–2I, 2M–2O and 2S–2U), in accordance with the base-to-apex gradient of hair cell differentiation along the cochlear spiral [9,52]. Importantly, the stereocilia of *je/je* mice did not show the usual large increases in diameter between P0 and P10. Instead, these stereocilia progressively shortened and disappeared (Figure 2H–2L and 2T–2X). This stereociliary degeneration was conspicuous on both outer hair cells (Figure 2K and 2L) and inner hair cells (Figure 2W and 2X) by P10, which is ~2–4 days before the onset of hearing in wild-type mice [53], and likely explains why *je/je* mice are deaf [43,47]. Interestingly, the average numbers of surface projections (stereocilia and microvillus-like structures) on the outer hair cells of *je/je* mice were similar to those in +/+ mice at P5, especially in the basal and middle regions of the cochlea (Table 1), and the projections approximated the "W" arrangement at P5 and P10 (Figure 2J and 2K). However, outer hair cells in the middle and basal regions of *je/je* mice lost ~70–75% of their surface projections between P5 and P10 (Figure 2L and Table 1), while the average numbers of surface projections did not change significantly during this same interval in +/+ mice (Figure 2D and 2F and Table 1). The loss of surface projections from the apical-region outer hair cells of *je/je* mice took place later, between P10 (Table 1) and P20 (Figure S2B). The extent of stereociliary shortening and loss was also strikingly evident for inner hair cells between P10 and P20 (Figure 2W and 2X, Figure 3B and Figure S2B and S2C), which assembled relatively large stereocilia in +/+ mice (Figure 2Q and 2R and Figure 3A). In addition, we detected some peculiar stereociliary defects on the inner hair cells of early postnatal *je/je* mice, including bulbous distal tips on the tallest row (Figure 3D) and branched, antler-like shapes for the shortest projections on the opposite side of the collection at P5 and P10 (Figure 3E–3G).

The degeneration of cochlear stereocilia in *je/je* mice continued so that by P20 and P40 only sparse, poorly organized remnants remained on both outer and inner hair cells (Figure 3B and 3C and Figure S2B and S2C). In addition, by P40 the apical surface of the outer hair cells in *je/je* mice had largely lost the flattened contour shape characteristic of outer hair cells [54] (compare Figure 3A and 3C), which it displayed earlier, at P10 (Figure 2K and 2L). Nevertheless, hair cells remained recognizable in these surface views owing to the regular row- or lattice-like position of their apical surface within the epithelium and the presence of stereociliary remnants on an otherwise smooth apical surface that was deficient in short microvilli relative to neighboring supporting cells (Figure 3B and 3C and Figure S2B). At P20 and P40, we began to detect positions within the epithelium from which hair cells appeared to be missing in surface views (Figure 3C, asterisk), often to be grown over by cells that resembled supporting cells because of their relatively dense collection of short microvilli (Figure S2C). It is unclear whether this reflected the loss or dedifferentiation of the hair cells or their retraction below the surface of the epithelium. This phenomenon was relatively rare in the apical region of the cochlea (Figure S2B), but was more pronounced in the middle region (Figure S2C) and greater still in the basal region (data not shown). By P90, few hair cells could be recognized in cochleae prepared from *je/je* mice, with the exception of some inner hair cells in the apical region (data not shown).

Unlike the situation in *je/je* mice, we found the stereocilia of adult +/*je* mice to appear similar to those in +/+ mice, even at 13 months of age (Figure 4A–4C). Importantly, we saw little or no

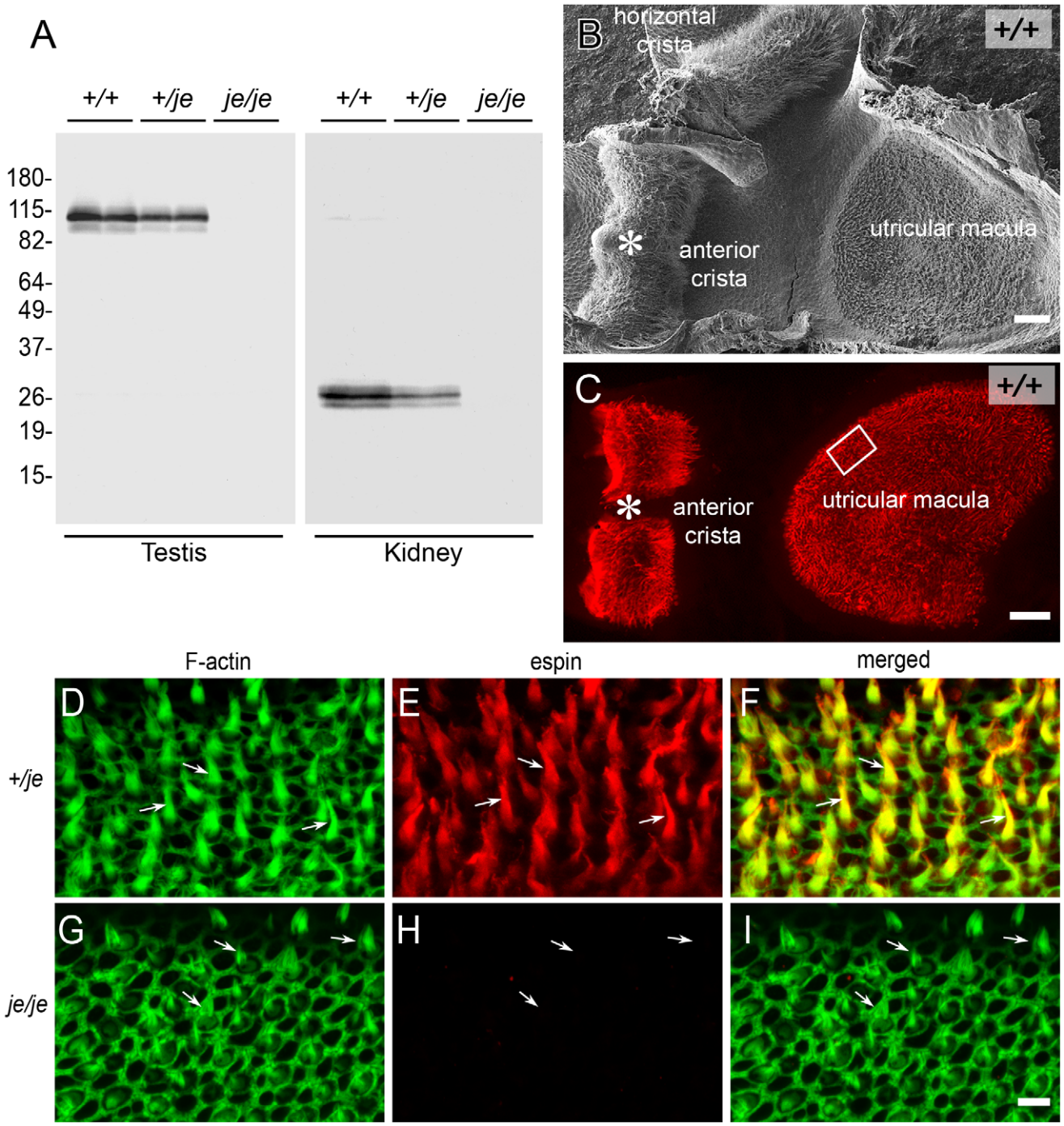

Figure 1. *je/je* mice lack espin proteins. (A) Western blots of duplicate samples of testis or kidney homogenate labeled with polyclonal espin antibody showing an absence of espin proteins in *je/je* mice and reduced espin levels in *+/je* mice compared to +/+ mice. Testis and kidney are rich sources of espin 1 (~105–110 kDa) and espin 4 (~22–28 kDa) isoforms, respectively. Numbers at left are apparent molecular mass in kDa. (B,C) Low-magnification views of vestibular system whole mounts isolated from P20 +/+ mice highlighting the utricular macula and anterior crista ampullaris as revealed by scanning electron microscopy (B) or fluorescence microscopy (C) after labeling with espin antibody (red). The labeled structures in the macula and crista in C are collections of espin-containing hair cell stereocilia, which give a rough or furry surface texture to the patches of hair cells observed by scanning electron microscopy (B). The shape of the macula appears different in B and C because in C the specimen has been flattened for mounting, whereas in B the macula displays concave-upward curvature. The specimen in B retains the adjacent horizontal crista ampullaris. The box in C shows the approximate location of the images of stereociliary collections shown in D-I. (D–I) Whole mounts of utricular maculae from P20 *+/je* (D–F) or *je/je* (G–I) mice labeled with espin antibody (red) and fluorescent phalloidin (green) to reveal F-actin, highlighting the collections of hair cell stereocilia (arrows). Stereociliary espins are detected in *+/je* mice (D–F), but not in *je/je* mice (G–I), even though many fluorescent phalloidin-labeled stereociliary collections, albeit shorter than in the *+/je* specimen, are evident (arrows in G–I). These images are taken from the region of the macula shown by the box in C, which corresponds to the lateral extrastriolar region. Scale bars, 50 μm (B,C) or 5 μm (D–I).
doi:10.1371/journal.pgen.1002032.g001

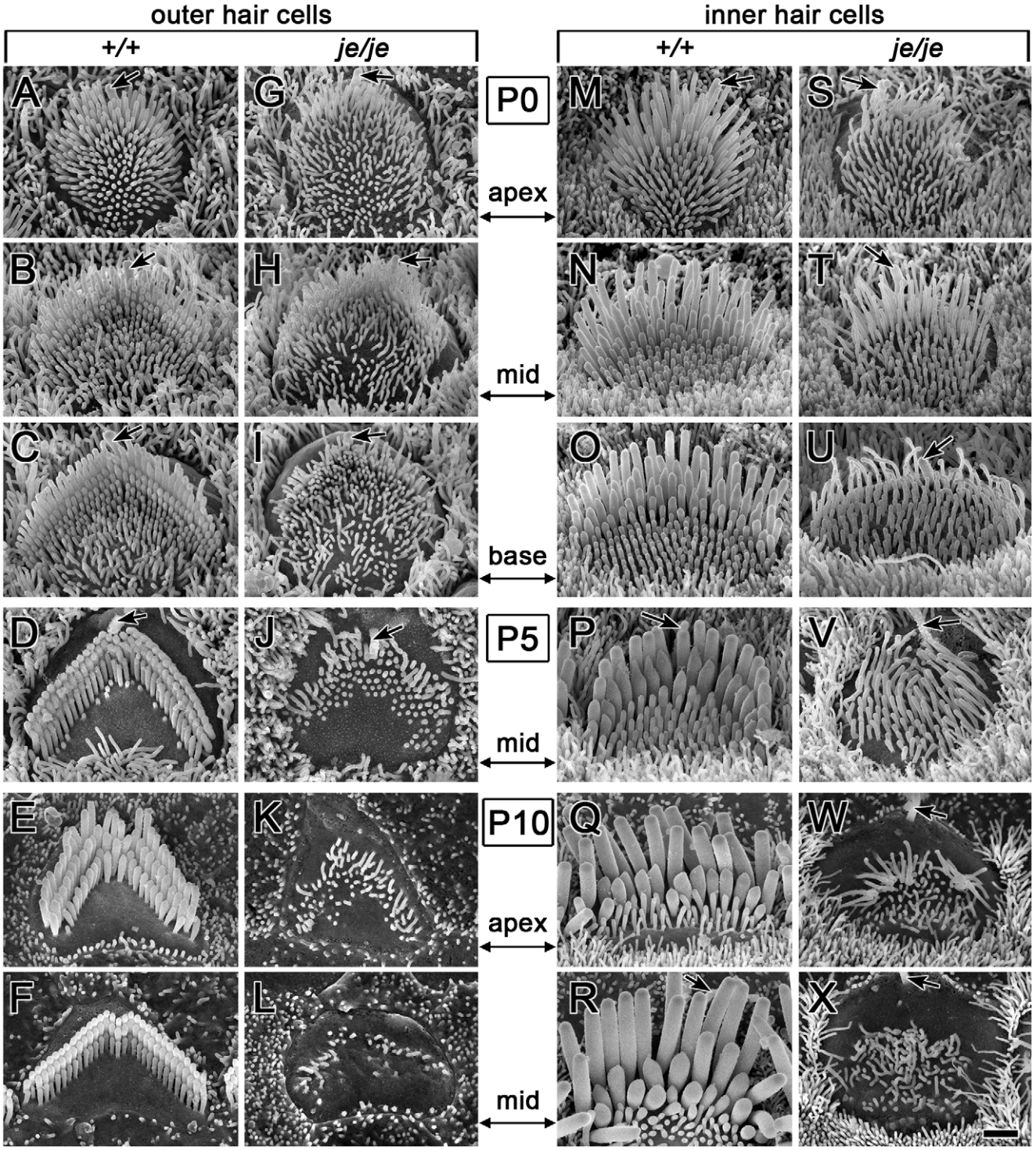

Figure 2. Morphogenesis defects and degeneration of cochlear hair cell stereocilia in *je/je* mice. Cochlear hair cells from +/+ mice and *je/je* mice are shown with the same magnification and orientation (abneural pole at top; kinocilium, arrow). (A–F,M–R) In +/+ mice, stereociliary morphogenesis for outer hair cells (A–F) and inner hair cells (M–R) involves an increase in diameter and length adjustments to form a staircase. For outer hair cells, it also includes organization of the stereocilia into the characteristic "W" shape (upside-down in figure) and the efficient clearance of other surface projections (microvilli) (D–F). A–C and M–O illustrate the base-apex gradient of stereocilium morphogenesis along the cochlear spiral. (G–L,S–X) In *je/je* mice, stereociliary morphogenesis is drastically impaired for outer hair cells (G–L) and inner hair cells (S–X). The surface projections in *je/je* mice look relatively similar to +/+ controls in length and length-gradation at the earliest stage examined, but are noticeably thinner (G,S). In *je/je* mice, stereociliary precursors fail to increase in diameter and elongate fully and instead shorten, bend or disappear (H–L and T–X). Scale bar, 1 μm.
doi:10.1371/journal.pgen.1002032.g002

Table 1. Average number of surface projections or missing stereocilia/outer hair cell[a].

		Base		mid		apex	
		P5	P10	P5	P10	P5	P10
Surface Projections	+/+	117±4	111±4	112±5	103±5	123±8	83±4
	+/je	111±5	107±4	108±4	102±6	110±6	82±4
	je/je	110±21	27±6*	110±10	31±7*	141±9	81±14
Missing stereocilia	+/+	-	0.5±0.8	-	0.1±0.3	-	0.8±0.8
	+/je	-	4.3±2.8*	-	1.1±1.2*	-	1.3±1.2

[a]Mean ± SD (n = 30 hair cells).
*Significantly different from +/+ control, $p<0.001$.
doi:10.1371/journal.pgen.1002032.t001

evidence for hair cell loss (Figure 4A–4C), even in the basal region of the cochlea (Figure 4C). This result differs from that of Sjöström and Anniko [46,47], who saw considerable loss of cochlear hair cells in aged jerker heterozygotes with an uncharacterized genetic background. However, we did notice in *+/je* mice occasional gaps in the shortest row of stereocilia on outer hair cells, indicative of missing stereocilia (Figure 4D and 4E). This effect was already evident at P10 and was most pronounced in the basal region of the cochlea, where the shortest row was missing an average of 4.3±2.8 stereocilia (range: 1–11) (Table 1 and Figure 4C–4E). Loss of one stereocilium or a small number of stereocilia from this row was also detected elsewhere along the cochlea in *+/je* mice (Figure 4B and Table 1), but not in +/+ mice (Figure 3A). Minimal effects in aged *+/je* mice were also noticed in hearing tests examining the auditory brainstem response. Although the average auditory brainstem response thresholds we measured for 13-month-old *+/je* mice appeared slightly elevated relative to those of 13-month-old +/+ mice at some of the frequencies tested, the differences were not statistically significant ($p>0.05$) (Figure 4F).

Vestibular system. We detected a related, yet distinct group of major stereociliary defects for the vestibular hair cells of *je/je* mice, including a different pattern of degeneration that varied according to region in the utricular macula and the cristae ampullares. The projections emanating from immature vestibular hair cells observed at P0 in the utricular maculae of *je/je* and +/+ mice were similar in length and length-gradation, but, as in the cochlea, those in *je/je* mice appeared thinner (Figure 5A and 5B). During morphogenesis, the stereociliary precursors of utricular hair cells in +/+ mice increased in diameter and elongated dramatically to form a prominent staircase consisting of ~6–10 rows of stereocilia (Figure 5A, 5C and 5G, Figure 6D, and Figure S3A and S3C). Although the counterparts in *je/je* mice elongated considerably beyond the precursor stage, they remained substantially thinner than those in +/+ mice, appeared to taper gradually in the proximal-to-distal direction and showed little or no differential elongation to form a staircase (Figure 5D, 5F, 5H and 5J, Figure 6E, and Figure S3B). At P5 and beyond, we detected a curious difference between stereocilia on hair cells in the striolar and extrastriolar regions of the utricular macula in *je/je* mice. Specifically, the striolar stereocilia of *je/je* mice exhibited a characteristic pattern of progressive stereociliary degeneration. In its initial phases, the striolar stereocilia were noticeably crooked and tapered (Figure 5J) and then appeared to collapse as a result of buckling in their proximal segment (Figure 5K). Later, the striolar stereocilia shortened and disappeared into the increasingly bulging apical surface of the hair cell (Figure 5K and Figure 6F). The stereocilia of striolar hair cells in +/+ mice did not show these defects (Figure S3C). By P40, the residual stereocilia remaining on the striolar hair cells of *je/je* mice displayed a distinctive "singed" appearance (Figure 6F), and the striolar region was sufficiently denuded to allow easy recognition of the stereocilium-deficient, degenerated zone in low-magnification images (Figure 6C, a higher magnification view of Figure 6A). The degeneration affected all vestibular hair cells within that region. The striolar region and the extrastriolar region both normally contain roughly similar numbers of type I and type II vestibular hair cells [10,55]. In contrast to the degeneration observed in the striolar region, stereocilia in the extrastriolar region of *je/je* mice, although thinner and shorter than those in +/+ mice (tallest: 5–6 μm long in *je/je* versus 12–13 μm long in +/+), were retained in larger numbers and persisted in upright form for a long period (Figure 5H and Figure 6E). Because of their slow rate of degeneration (Figure 6E) and because they contain espin proteins in +/+ and *+/je* mice (Figure 1C and 1E), we regard the stereocilia on the extrastriolar hair cells of *je/je* mice at P10–P40 as exemplars of espin protein-null stereocilia suitable for side-by-side comparison with wild type (compare Figure 5G and 5H or Figure 6D and 6E). Unlike the situation in +/+ mice, where definitive staircases could be observed (Figure 5C and 5G and Figure 6D), stereocilia on the extrastriolar hair cells of *je/je* mice were more similar in length, with little or no recognizable staircase (Figure 5D, 5F and 5H, and Figure 6E). The average height measured for these extrastriolar stereociliary collections in *je/je* mice remained relatively constant at ~4 μm from P0 through P60 (Figure 5E). Although their closely packed arrangement gave the impression that these thin stereocilia might be present in greater numbers, we counted similar numbers of stereocilia on the extrastriolar hair cells of *je/je* and +/+ mice at P20 (38±4 for *je/je* versus 40±4 for +/+; mean±SD, n = 15–18 cells; unpaired t-test, p = 0.1). By P60 and P90, the stereocilia of the extrastriolar hair cells in *je/je* mice were noticeably thinner than at P20 or P40 in their proximal segment, and many had shortened and disappeared (Figure S3G–S3J).

We detected an analogous group of stereociliary defects for vestibular hair cells in the cristae ampullares of *je/je* mice, however the greater lengths of these stereocilia and their extensive splaying and entanglement made them more difficult to analyze. Stereocilia in the cristae of *je/je* mice elongated considerably beyond the immature stage, especially in the peripheral zone (Figure 7E–7G, 7I and 7J, and Figure S3D–S3F), but they remained thinner, shorter and more tapered than in +/+ mice (Figure 7A–7K and Figure S3D–S3F), and there was relatively little differential elongation to form a staircase (Figure 7E–7G and 7I–K and Figure S3D–S3F). By analogy to the situation in utricular maculae, stereocilia in the cristae of *je/je* mice showed region-dependent degeneration, with those in the central zone showing more pronounced degeneration than those in the peripheral zone (compare Figure 7B and 7C with Figure 7E–7G, 7I and 7J). Notably, the central zone stereocilia buckled and collapsed (Figure 7C) like those in the striolar region of the utricular macula (Figure 5K). In contrast, stereocilia in the peripheral zone of *je/je* mice, although thinner and shorter than those in +/+ mice (tallest: 5–8 μm long in *je/je* versus 22–30 μm long in +/+), were maintained in a more upright position for a longer period (Figure 7E–7G, 7I and 7J). The depletion of stereocilia in the central zone relative to the surrounding peripheral zone could be detected at low magnification, but was more difficult to discern than in the striolar region owing to the presence of prominent long kinocilia (Figure 6B). Despite the similarities between stereocilia in the peripheral zone of cristae and the extrastriolar region of

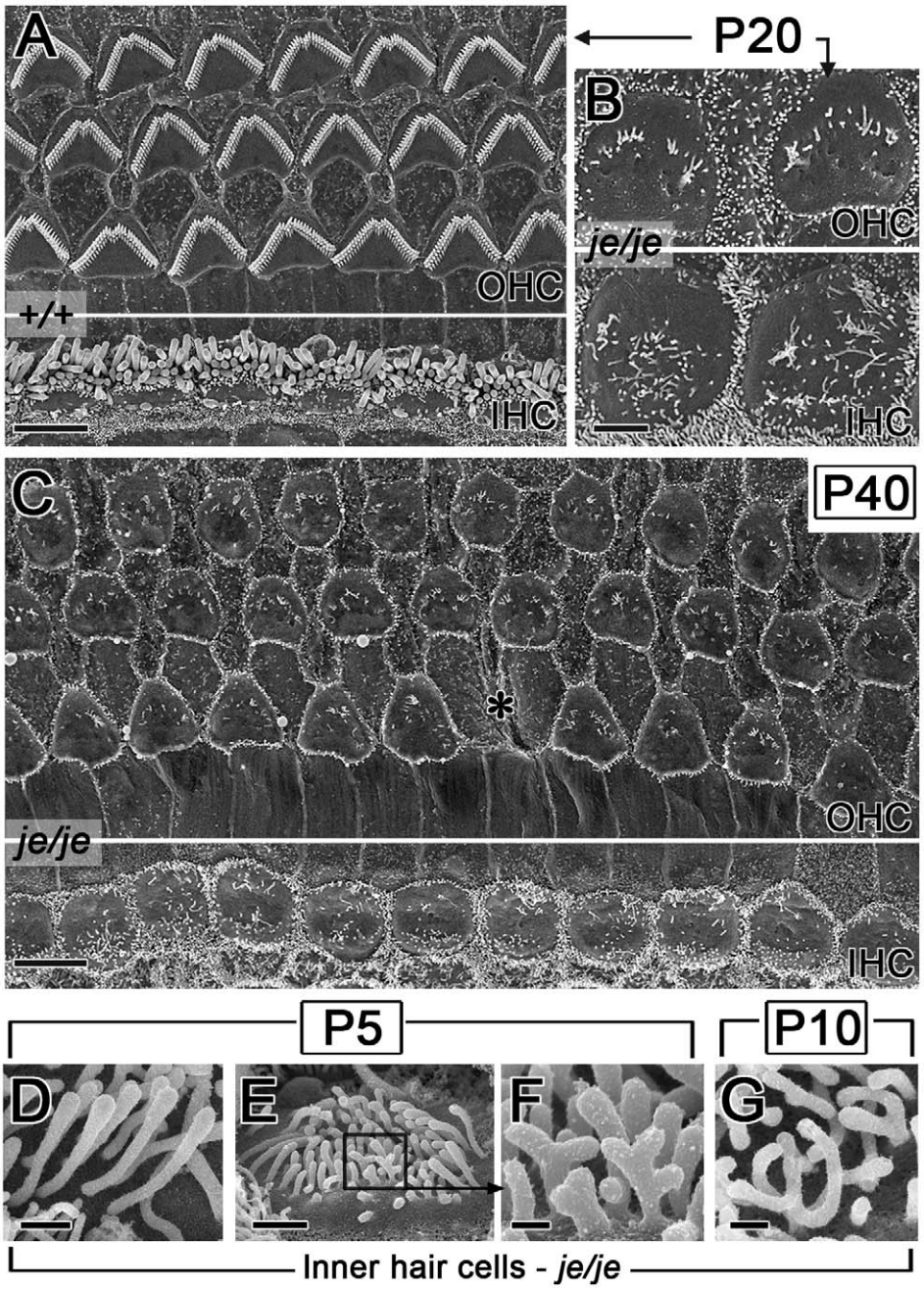

Figure 3. Advanced stereociliary degeneration on cochlear hair cells and peculiar stereociliary defects on inner hair cells. (A–C) Stereociliary degeneration involving shortening and disappearance (see Figure 2) progresses for the outer hair cells (OHC) and the inner hair cells (IHC) of *je/je* mice. By P20 and P40, only sparse, disorganized collections of small stereociliary remnants remain (B,C). The middle region of the cochlea is shown. Panel A shows the corresponding region in P20 +/+ mice. Asterisk in C, position missing an outer hair cell. (D–G) Higher magnification reveals peculiar defects in *je/je* mice at P5 and P10, including bulbous tips for inner hair cell stereocilia in the tallest row (D) and branched, antler-like surface projections on the opposite (neural) face of the collection (E–G). F is a higher-magnification view of the box in E. Scale bars, 5 μm (A,C), 2 μm (B), 0.5 μm (D), 1 μm (E) or 0.2 μm (F,G).
doi:10.1371/journal.pgen.1002032.g003

utricular maculae in *je/je* mice, we did notice some differences. Peripheral zone stereocilia were noticeably thinner at P40 than at P5 (Figure 7F and 7J). In addition, ~50% (69/146) of the peripheral zone hair cells examined in P20 *je/je* mice showed elbow-like bends in the proximal segment of their stereocilia (Figure S3D–S3F, arrowheads), and ~10% (13/146) had a stereocilium that extended a long, thin distal process in association with the kinocilium (Figure 7K and Figure S3D).

Stereociliary dimensions

Cochlea. To gain a better understanding of the roles of espins in the morphogenesis of the stereociliary parallel actin bundle, we measured the dimensions of stereocilia in +/+, +/*je* and *je/je* mice on selected postnatal days, focusing on the times before degeneration became pronounced in *je/je* mice. Because the stereociliary plasma membrane remains in close proximity to the parallel actin bundle during morphogenesis [6], we used these

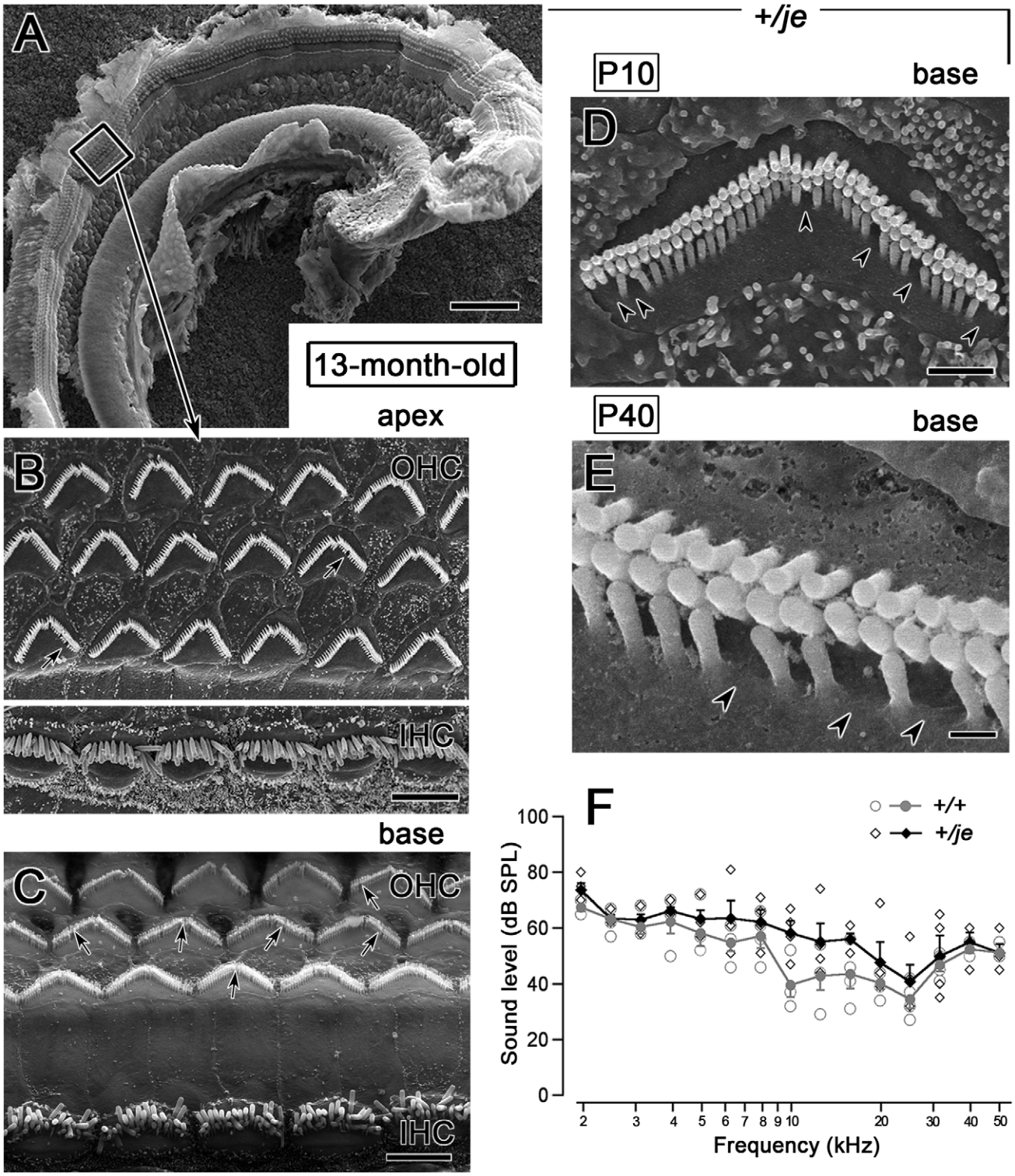

Figure 4. Minimal stereociliary defects, hair cell loss, and auditory brainstem response shifts in aged *+/je* mice. (A–C) The stereocilia of inner and outer hair cells in 13-month-old *+/je* mice look similar to those in +/+ mice. At low magnification (A), ridges representing collections of stereocilia on the three rows of outer hair cells and single row of inner hair cells can be traced without interruption throughout the entire apical half-turn of the cochlea. The box in A is shown at higher magnification in B and reveals collections of stereocilia similar to those in +/+ mice (Figure 3A). C shows the basal region, where there is also no evidence for hair cell loss, however arrows in B and C show examples of missing stereocilia. Scale bars, 100 μm (A) or 5 μm (B,C). (D,E) Higher magnification views of outer hair cell stereocilia in P10 *+/je* mice showing examples of stereocilia missing from the shortest row of stereocilia (arrowheads). Scale bars, 1 μm (D) or 0.2 μm (E). (F) The auditory brainstem response curve for 13-month-old *+/je* mice is similar to that for age-matched +/+ mice. Although thresholds for aged *+/je* mice appear slightly higher, the differences are not statistically significant ($p>0.05$). Open symbols are measurements from individual animals, and filled symbols are means.
doi:10.1371/journal.pgen.1002032.g004

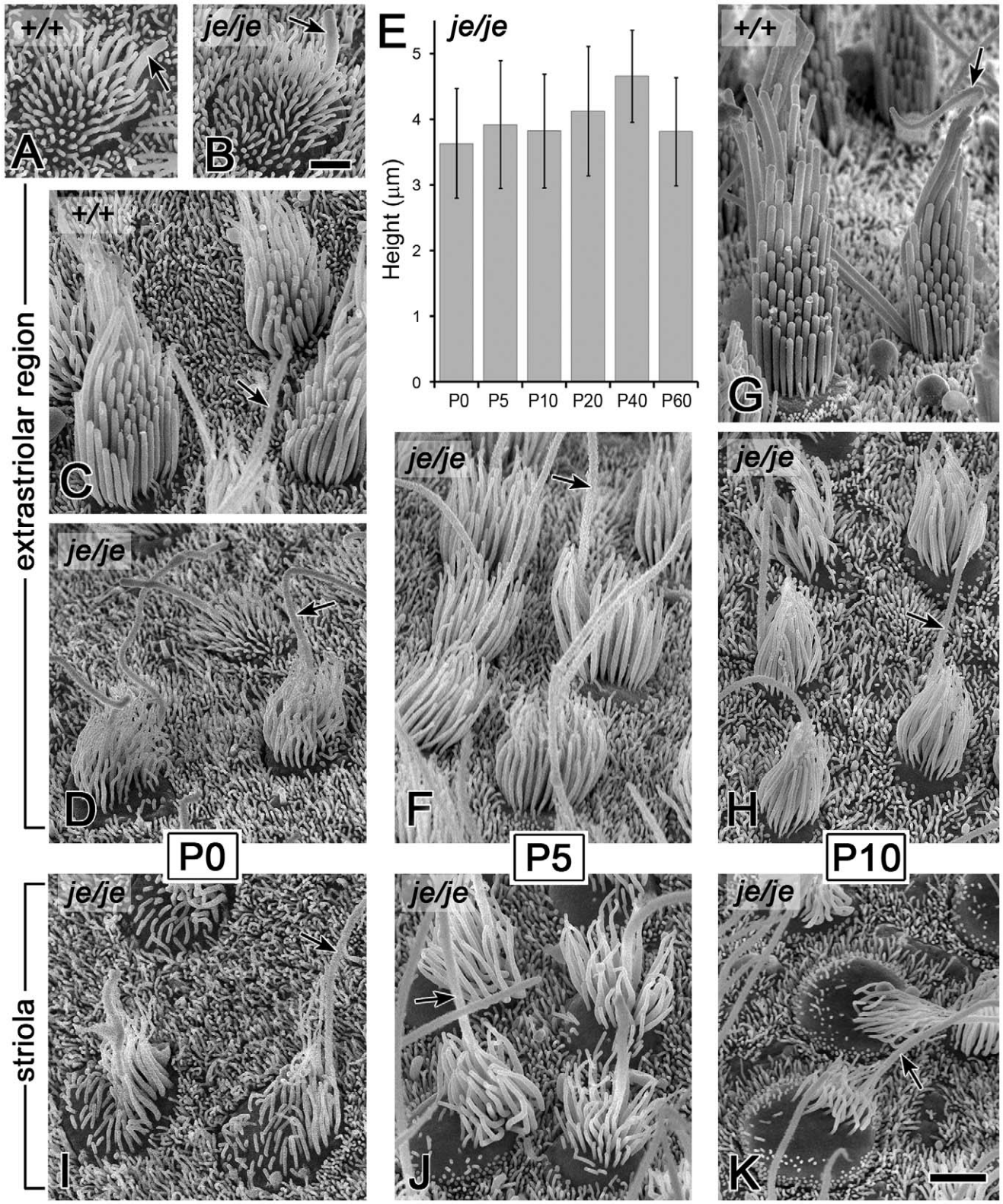

Figure 5. Morphogenesis defects and degeneration of vestibular hair cell stereocilia in utricular maculae of *je/je* mice. Extrastriolar and striolar regions of utricular maculae are shown (kinocilium, arrow). (A,B) At P0 the surface projections of immature utricular hair cells in *je/je* mice (B) look similar to those in +/+ mice (A) in length and length-gradation, but those in *je/je* mice appear thinner. (C,G) During stereociliary morphogenesis in +/+ mice, stereocilia increase in diameter and undergo differential elongation to form a relatively tall staircase. (D–F,H–K) Stereociliary morphogenesis is significantly impaired in *je/je* mice. Stereocilia are much thinner and appear to taper gradually in the proximal-to-distal direction, and there is little or no differential elongation to form a staircase. Additionally, in the striolar region, progressive stereociliary degeneration is evident: stereocilia become crooked and appear to collapse by buckling in their proximal segment (J,K). In contrast, stereocilia in the extrastriolar region attain a length that is approximately one-half that of the tallest stereocilia observed on the extrastriolar hair cells of +/+ mice and remain

upright for a longer period of time (D,F,H). The average height of the stereociliary collection in *je/je* mice changes little between P0 and P60 (E). Examples of stereocilia on the striolar hair cells of +/+ mice are shown in Figure S3A and S3C. Scale bars, 1 μm (A,B) or 2 μm (C,D,F–K).
doi:10.1371/journal.pgen.1002032.g005

measurements to infer changes in the dimensions of the underlying parallel actin bundle scaffold. In the cochlea, we measured stereocilia at P0 and P5, because degeneration was already prominent by P10 (Figure 2L and 2X and Figure 8I and 8S). When measuring length, we focused on the tallest stereocilia, in effect asking the question of how long stereocilia can become in mice of the three genotypes. Even though we detected some noteworthy differences in stereociliary length, the most substantial and consistent differences we observed were in the category of stereociliary width.

In the cochleae of *je/je* mice, average stereociliary width did not increase beyond ~0.12–0.14 μm and, thus was significantly smaller than in +/+ or +/*je* mice for outer and inner hair cells in all three regions of the cochlea (Figure 8 and Figure 9). In +/+ mice, the stereocilia of inner hair cells attained larger diameters than those of outer hair cells (Figure 8A–8C and 8J–8L and Figure 9A and 9B). Thus, the most striking differences in *je/je* mice were observed for the stereocilia of inner hair cells, which were ~50–60% thinner than those in +/+ mice at P0 and P5 (Figure 8J–8L and 8P–8S and Figure 9B). The stereocilia of outer hair cells in *je/je* mice were ~30–40% thinner than those in +/+ mice (Figure 8A–8C and 8G–8I and Figure 9A). Interestingly, the stereocilia of +/*je* mice were significantly thinner than those in +/+ control mice at P0, except on inner hair cells in the apical region (Figure 8A, 8D, 8J and 8M and Figure 9A and 9B). This unexpected difference in width for +/*je* mice was temporary. By P5 and beyond, stereociliary width had increased significantly for +/+ mice and +/*je* mice in all cochlear locations ($p<0.001$), and the stereocilia in +/*je* mice had become similar in width to those in +/+ mice (Figure 8E, 8F, 8N and 8O and Figure 9A and 9B). Remarkably, even the stereocilia of *je/je* mice showed a significant increase in width (37–51%; $p<0.001$) between P0 and P5 in all three cochlear regions (Figure 9A and 9B).

Stereociliary length was different from width in that it did not vary in such a regular way according to genotype or postnatal day. In some situations, the stereocilia of *je/je* mice were shorter than those in +/+ mice. For example, at P0 the tallest stereocilia on the outer hair cells of *je/je* mice were significantly (25–33%) shorter than those in +/+ mice in all three cochlear regions examined (Figure 8A and 8G and Figure 10A). They were also shorter at P5, except in the basal region (Figure 10A), but the difference was smaller (18–21%). In the basal region of the cochlea, a different trend was overriding: the tallest stereocilia on outer hair cells in mice of all three genotypes exhibited a significant, ~50%, shortening compared to P0 ($p<0.001$) to become of similar length (Figure 8A–8I and Figure 10A). Although the early postnatal shortening of outer hair cell stereocilia in the basal region of wild-type mice was noted previously [56], we also observed this type of shortening for outer hair cells in the middle region of the cochlea (Figure 10A). The situation for inner hair cells was even more complicated. The tallest stereocilia on inner hair cells in *je/je* mice were significantly (38–49%) shorter than those in +/+ mice, but only in the middle and apical regions at P0 (Figure 10B). Those in the apical region were also significantly (31%) shorter at P5 (Figure 10B). The stereocilia of *je/je* mice were not always shorter, however. At P5, the tallest stereocilia of inner hair cells in the basal region of *je/je* mice, although abnormally thin, were slightly, albeit significantly, longer than those in +/+ mice (Figure 8K and 8R and Figure 10B). As with our width measurements, we detected some significant differences in stereociliary length between +/*je* and +/+ mice at P0: the cochlear stereocilia of P0 +/*je* mice were of intermediate length and significantly shorter than their +/+ counterparts on outer hair cells in the middle region (Figure 10A) and on inner hair cells in the apical region (Figure 10B). These length differences were also transitory, because at P5 and beyond the cochlear stereocilia of +/*je* and +/+ mice were of similar length (Figure 10A and 10B).

Utricular macula. Differences in stereociliary width and length were shown to special advantage by hair cells in the extrastriolar region of utricular maculae. Because these stereocilia were preserved in upright form for a longer time than in the cochlea (Figure 6E), we could make measurements at additional time points to increase precision and better uncover developmental trends. In addition, these stereocilia were longer than in the cochlea, allowing width measurements to be made at additional increments along the length of stereocilia, but not as long as in the cristae ampullares, where excessive length, splaying, and entanglement precluded the quantification of stereociliary dimensions. The collection of stereocilia on the extrastriolar utricular hair cells of *je/je* mice maintained an average height in the 3.5–4.5 μm range from P0 through P60 (Figure 5E). From P5 through P40, the tallest stereocilia were ~6 μm long, compared to 12–13 μm long in +/+ and +/*je* mice (Figure 11A–11C and Figure S3G and S3J). Importantly, from P0 through P20 stereociliary width was significantly smaller in *je/je* mice compared to +/+ mice at every 1–μm interval along the length of the stereocilium, except at the base, where the tapered region emanated from the apical surface of the hair cell (Figure 11A–11C). Notably, espins are not detected in stereociliary rootlets [36]. Although the extrastriolar stereocilia of *je/je* mice eventually became even thinner and shorter at P60 and P90 (Figure S3G–S3J), there was little or no change in their width profiles between P0 and P40 (Figure 11C and Figure S3J). Thus, from P5 through P40, stereociliary width in *je/je* mice was reduced 50–60% relative to +/+ mice (Figure 11C and Figure S3J), like we observed for inner hair cells at P0 and P5 (Figure 9B), however the stereocilia showed a gradual taper, appearing widest ~1 μm from the base and thinner toward the distal tip (Figure 11C and Figure S3J).

Tapered stereocilia in +/*je* mice

Examination of the stereocilia of vestibular hair cells in +/*je* mice revealed an unexpected developmental defect: transient tapering. As shown in Figure 11C, the width of stereocilia on the extrastriolar hair cells of +/*je* mice (dashed line) was intermediate to those in *je/je* and +/+ mice at P0, but eventually increased to become highly similar to that in +/+ mice by P20. What is remarkable is that this increase in stereociliary width was gradual and took place first in the proximal part of stereocilia and later in the distal part, resulting in stereocilia that were transiently tapered from P0 through P10 (Figure 11C and Figure 12A). A similar gradual tapering of stereocilia was observed in the peripheral zone of the cristae ampullares in +/*je* mice at P5 (Figure 12D). Stereociliary tapering, but of a more extreme and abrupt nature, was also seen in the central zone of the cristae ampullares in +/*je* mice at P0, P5 and P10 (P5 shown in Figure 12B and 12C). The distal segment of these stereocilia was often dramatically thinner than the proximal segment, giving the appearance of a candle with a wick (Figure 12B and 12C). Notably, up to a length of ~4 μm, the width of the proximal segment of these stereocilia was similar to that in +/+ mice (compare Figure 12B and Figure 7A). By P20,

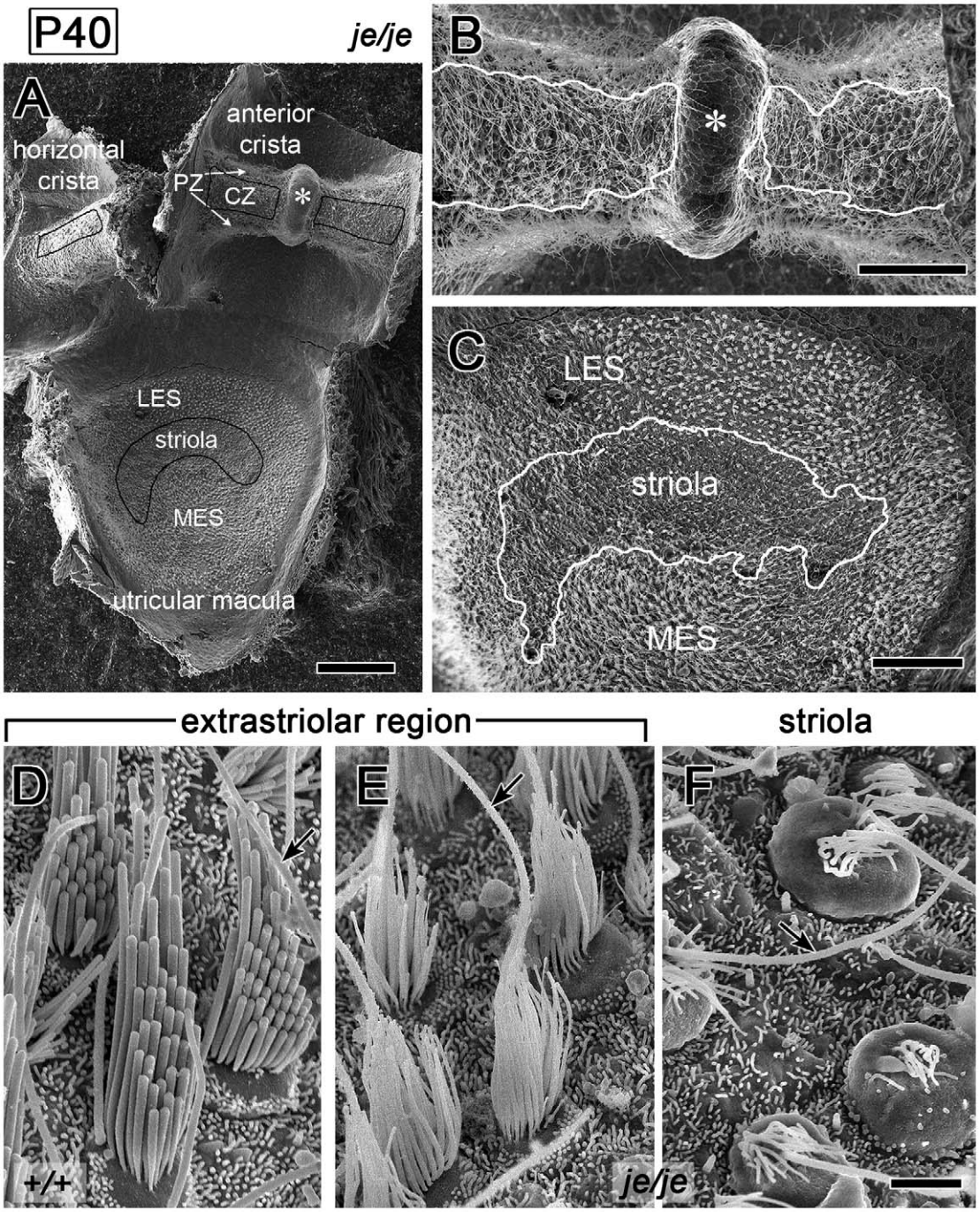

Figure 6. Regional differences in the fate of stereocilia on vestibular hair cells in *je/je* mice. (A) Specimen from a P40 *je/je* mouse showing the utricular macula and horizontal and anterior cristae ampullares. The black lines approximately outline the striolar region of the macula and the central zones (CZ) of the cristae. The extrastriolar region of the macula lies outside the striolar region and includes lateral extrastriolar (LES) and medial extrastriolar (MES) regions. The peripheral zone (PZ) of each crista lies outside the central zone. The anterior crista is divided by the eminentia cruciatum (asterisk), which is also devoid of hair cells in +/+ mice. (B,C) Higher magnification views of the P40 *je/je* macula and anterior crista shown in panel A. White lines enclose the relatively denuded regions showing extensive stereociliary degeneration, which approximate the striolar region of the macula (C) and the central zone of the crista (B). The degeneration of stereocilia in the striolar region is easy to see at this magnification (C). A depletion of stereocilia in the central zone of the crista relative to the surrounding peripheral zone can also be detected, but is more difficult to discern because of the long kinocilia (B). (D–F) Differences in stereocilia on extrastriolar (E) and striolar (F) hair cells in the utricular macula of P40 *je/je* mice. Stereocilia on striolar hair cells (F) collapse and shorten, appearing ''singed,'' and the hair cells bulge out of the epithelium. Stereocilia on extrastriolar hair cells (E), although thinner and shorter than those in +/+ mice (D), remain upright even at P40. Scale bars, 100 μm (A), 50 μm (B,C) or 2 μm (D–F).

doi:10.1371/journal.pgen.1002032.g006

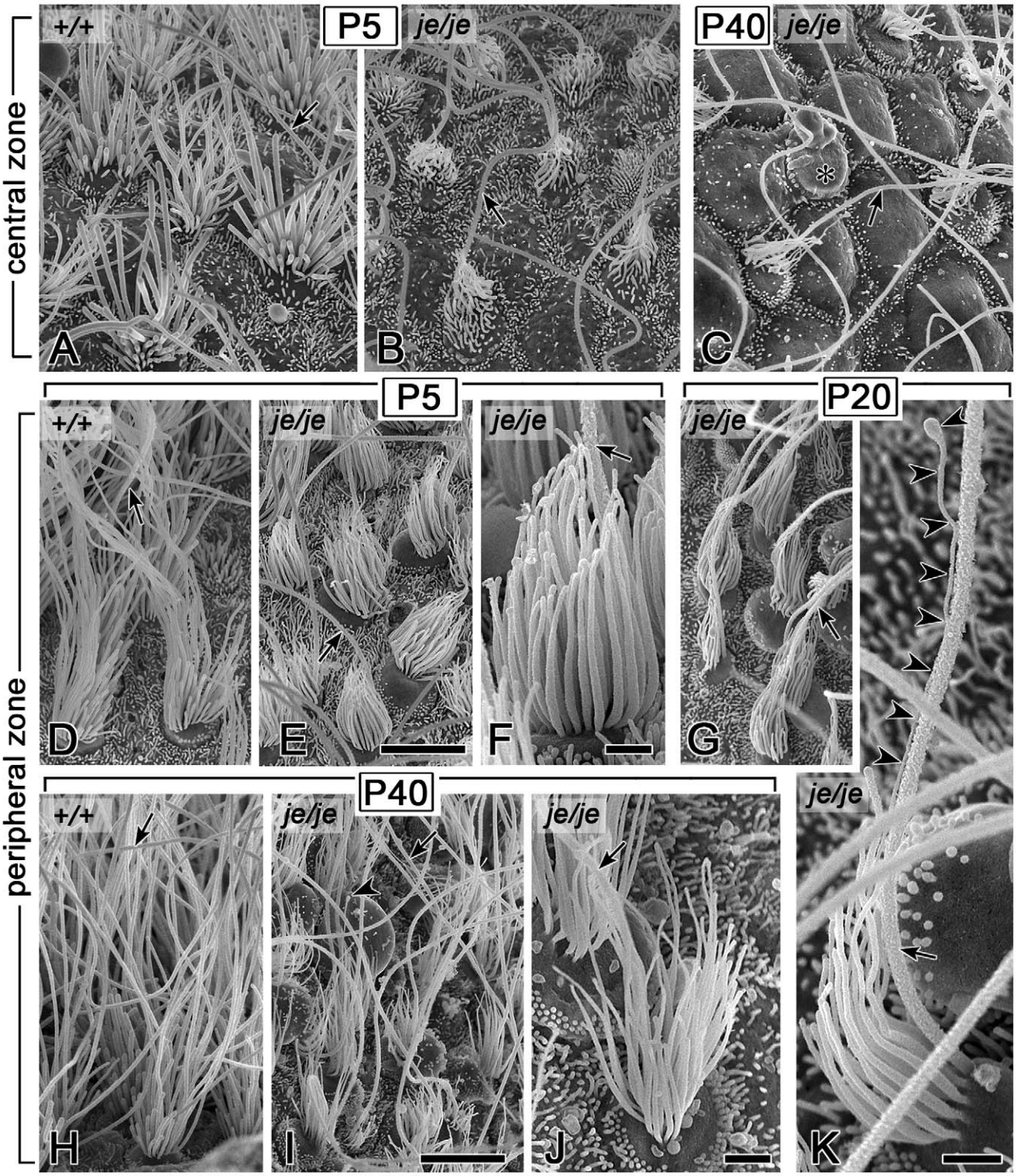

Figure 7. Morphogenesis defects and degeneration of vestibular hair cell stereocilia in cristae ampullares of *je/je* mice. Kinocilium, arrow. (A–C) Stereocilia in the central zone of P5 *je/je* mice (B) are shorter, thinner, and more crooked than those in P5 +/+ mice (A). By P40, stereocilia in the central zone are collapsed, and hair cells bulge out from the epithelium (C). Asterisk, probable hair cell, on the basis of size, devoid of stereocilia and showing a large bleb. (D–K) Stereocilia in the peripheral zone of *je/je* mice at P5 (E,F), P20 (G,K) and P40 (I,J), although thinner than those in +/+ mice (D,H), remain more upright. At P40, peripheral zone stereocilia in *je/je* mice (I,J) appear thinner than at P5 (E,F) (compare F and J). (K) Stereociliary collection in the peripheral zone of a P20 *je/je* mouse showing a stereocilium that extends a very thin distal process (arrowheads) in close association with the kinocilium (see also Figure S3D). Scale bars, 5 μm (A–E,G–I) or 1 μm (F,J,K).
doi:10.1371/journal.pgen.1002032.g007

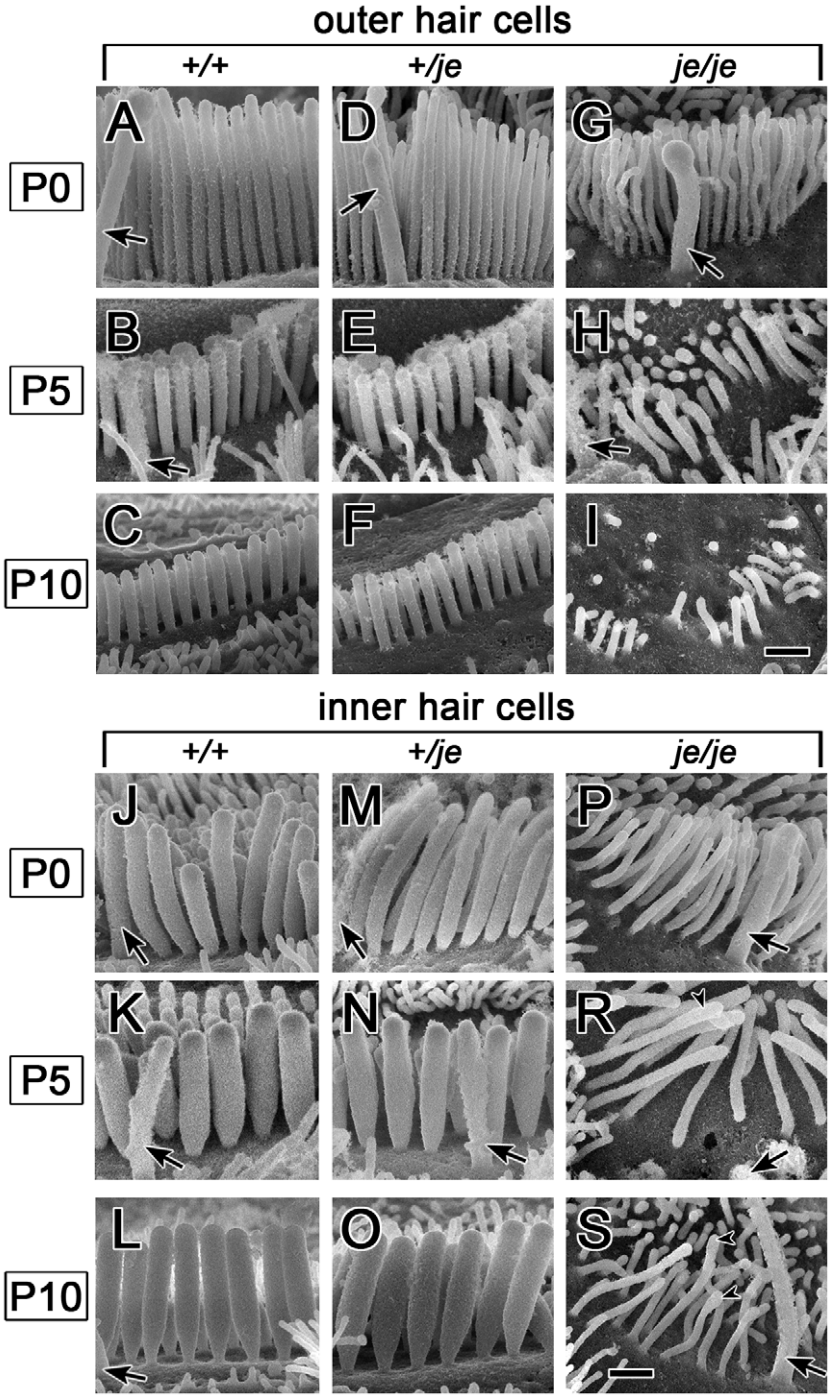

Figure 8. Stereociliary dimensions for basal-region cochlear hair cells in early postnatal *+/+*, *+/je*, and *je/je* mice. Views of basal-region stereocilia from the abneural side are shown (kinocilium, arrow). (A–I) Outer hair cells. Stereocilia in *je/je* mice (G–I) are thinner than those in +/+ mice (A–C), while those in *+/je* mice are intermediate in width at P0 (D). Stereocilia shorten during early postnatal development for all genotypes (A–I), but pronounced shortening leading to disappearance is evident only in *je/je* mice (G–I). At P5 and beyond, the stereocilia in +/+ mice and *+/je* mice appear similar (B,C,E,F). (J–S) Inner hair cells. Stereocilia in *je/je* mice (P–S) are substantially thinner than those in P5 +/+ mice (J–L), while those in *+/je* mice are intermediate in width at P0 (M). Unexpectedly, the stereocilia in P5 *je/je* mice (R) are slightly longer than those in +/+ and *+/je* mice (K,N). At P5 and beyond, stereocilia in +/+ mice and *+/je* mice appear similar (K,L,N,O). Arrowheads in R and S point to bulbous distal tips of stereocilia. Scale bars, 0.5 μm.
doi:10.1371/journal.pgen.1002032.g008

few of these extremely thin distal segments remained (Figure 12F), suggesting that most had grown longer and widened sufficiently to match their proximal segments. Also evident in the central zone of P5 +/*je* mice were stereocilia with eccentric protruding distal tips, which were suggestive of intermediates caught in a relatively early stage of additional elongation (Figure 12E, arrowheads).

A close scrutiny of inner hair cells also revealed the transient tapering of stereocilia in +/*je* mice. This tapering was especially

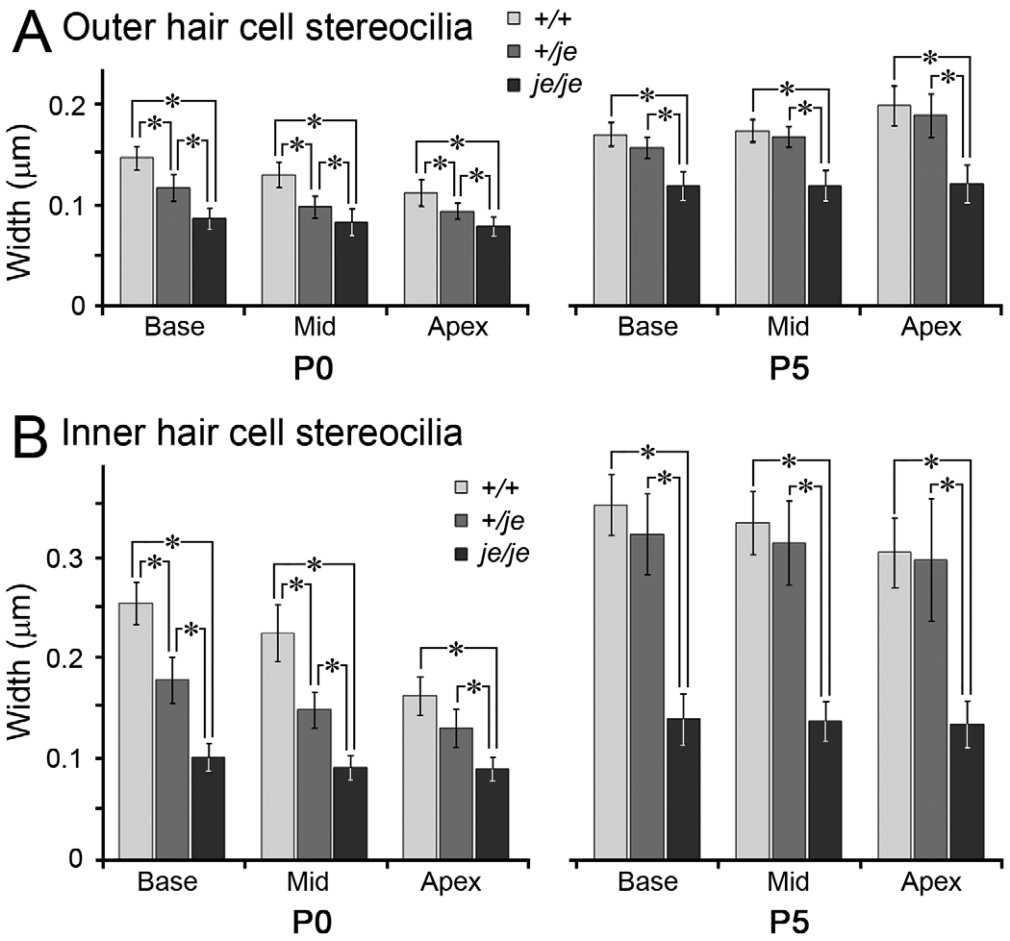

Figure 9. Stereociliary width measurements for cochlear hair cells in early postnatal *+/+*, *+/je*, and *je/je* mice. Width measurements for 150 (P0) or 100 (P5) stereocilia on hair cells of the designated type (outer or inner), cochlear location and genotype are plotted as mean ± SD (*, $p<0.001$). (A,B) Stereocilia on outer (A) and inner (B) hair cells in *je/je* mice are significantly thinner than those in +/+ mice in all cochlear regions at P0 and P5, while those in *+/je* mice are intermediate in width and significantly different from those in +/+ and *je/je* mice at P0, except on inner hair cells in the apical region. The stereocilia of outer and inner hair cells in all three genotypes and cochlear regions show significant increases in width between P0 and P5 ($p<0.001$).
doi:10.1371/journal.pgen.1002032.g009

evident for stereocilia in the tallest row in the apical region of the cochlea at P5 (Figure 13D), but was also detected in the middle region (Figure 13B). The tapering was not detected in +/+ mice (Figure 13A, 13C, 13E and 13G). In the basal and middle regions of the cochlea, the tapering was no longer detected at P10 (Figure 13F), but it was still partially evident in the apical region (Figure 13H). By P20, the tapering of the tallest stereocilia was only observed in the extreme apical region of the cochlea (>95% from cochlear base). In this region, a partial tapering was still observed at P20 (Figure 13J and 13K) and even at 8 months of age (Figure 13L), but not in +/+ mice (Figure 13I).

Discussion

We detected a unique and informative group of major stereociliary defects in the CBA/CaJ congenic jerker mouse line. Because of its chosen genetic background, we have increased confidence that these defects reflect the absence of espins. In general, the lack of espin proteins resulted in stereocilia that were abnormally thin and short and prone to degeneration, characteristics which fit remarkably well with the biological activities displayed by espins in vitro and in transfected cells. Our major unexpected findings were the primacy of the effects on stereocilium width, the transient tapering of stereocilia in *+/je* mice, which brought to light previously unrecognized assembly steps and intermediates, and the region-specific degeneration of stereocilia in *je/je* mice. Beyond demonstrating that espins are required for the morphogenesis and stabilization of hair cell stereocilia, our results clear up some misconceptions about the jerker mutation and offer new insights into the mechanisms of stereociliary parallel actin bundle morphogenesis and the crucial roles played by espins.

Width defect and appositional growth

The most consistent morphogenesis defect we observed in *je/je* mice was the failure of stereocilia to increase in mean diameter beyond ~0.10–0.14 μm. Because stereocilia grow to different diameters in +/+ mice, this made the stereocilia of *je/je* mice ~50–60% thinner than wild type for inner hair cells and utricular hair cells and ~30–40% thinner than wild type for outer hair cells. The increase in stereocilium diameter during morphogenesis is presumed to reflect the appositional growth of the parallel actin bundle scaffold at the core, in which additional actin filaments are added at the periphery of the existing parallel actin bundle [4–6]. A 50–60% decrease in stereocilium diameter translates into a 75–

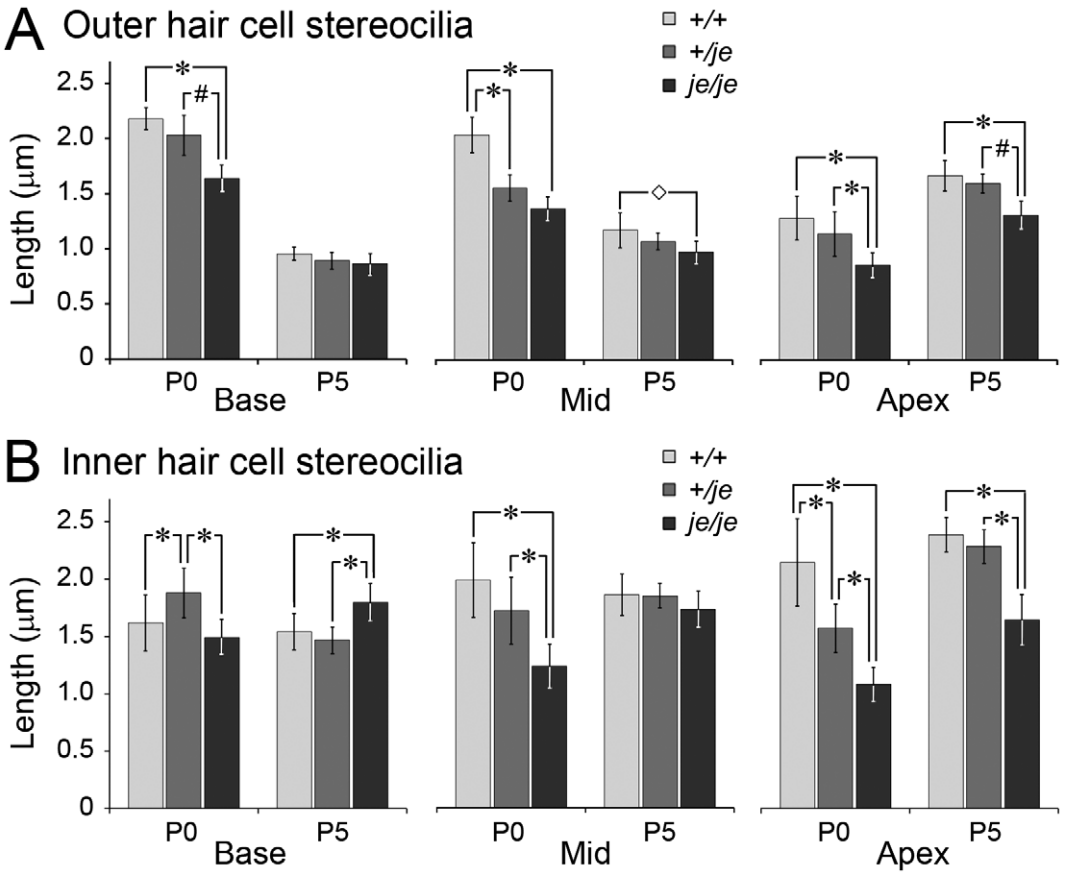

Figure 10. Stereociliary length measurements for cochlear hair cells in early postnatal *+/+*, *+/je*, and *je/je* mice. Length measurements for 120 (P0) or 80 (P5) tallest stereocilia on hair cells of the designated type (outer or inner), cochlear location and genotype are plotted as mean ± SD (*, $p<0.001$; #, $p<0.01$; ◇, $p<0.05$). (A) Outer hair cells. The tallest stereocilia in *je/je* mice are significantly shorter than those in +/+ mice for all conditions examined, except at P5 in the base. Note the shortening of stereocilia between P0 and P5 for all three genotypes in basal and middle regions ($p<0.001$). At P5 the tallest stereocilia in *+/je* mice are similar in length to those in +/+ mice. (B) Inner hair cells. The relationship between genotype and stereocilium length is not straightforward. While some situations (P0 Mid and Apex and P5 Apex) show the tallest stereocilia in *je/je* mice to be significantly shorter than those in +/+ mice, other situations (P0 Base and P5 Mid) show little difference. In addition, the tallest stereocilia in *je/je* mice are slightly, yet significantly, longer than those in +/+ mice in the basal region at P5. Note that, at P0, the tallest stereocilia on inner hair cells in *+/je* mice are significantly shorter than those in +/+ mice in the apical region, but significantly longer than those in +/+ mice in the basal region. At P5, the tallest stereocilia in *+/je* mice are similar in length to those in +/+ mice.
doi:10.1371/journal.pgen.1002032.g010

84% decrease in cross-sectional area. Assuming that the actin filaments in the abnormally thin projections maintain the standard ~12–13 nm parallel actin bundle interfilament spacing [30,31], the parallel actin bundle scaffold of *je/je* mouse hair cell stereocilia could contain as little as 16–25% of the number of actin filaments found in the stereocilia of +/+ mice. The abnormally thin utricular stereocilia in P20 *je/je* mice labeled with fluorescent phalloidin (Figure 1G), suggesting that they contain actin filaments, a conclusion that has been confirmed by transmission electron microscopy (GS and JRB, unpublished results). Definitive assessments of the numbers, continuity and packing of these actin filaments will come from systematic serial-section analyses. The present examination of stereociliary dimensions suggests that espin proteins are required to increase the diameter of the stereociliary parallel actin bundle beyond a limiting value. A role in the appositional growth of the stereociliary parallel actin bundle would be entirely consistent with the espins' activity as actin-bundling proteins that can efficiently cross-link actin filaments into parallel actin bundles in vitro [28–30] and with the immunocytochemical localization of espins to hair cell stereocilia throughout the process of stereociliary morphogenesis [35,37].

Transient tapering in *+/je* mice and assembly intermediates

Defects in the appositional growth of the parallel actin bundle could also explain the transient stereociliary tapering we discovered in young *+/je* mice. This novel phenotype is most likely a sign of haploinsufficiency, in which espin protein levels are limiting. The transient tapering is consistent with a slowing in the appositional growth of the stereociliary parallel actin bundle, and we propose that this slowing revealed some exclusive views of assembly intermediates and steps that are difficult to resolve in +/+ mice. For example, the direction of the taper and its subsequent filling suggest that the appositional growth of the parallel actin bundle proceeds in a proximal-to-distal direction and, thus, likely involves the barbed-end elongation of shorter actin filaments positioned in the peripheral layers of a wider, more proximal segment of the core bundle. How could reducing espin levels by approximately one-half slow the appositional growth of the parallel actin bundle? Beyond cross-linking actin filaments into parallel actin bundles [28–30], espins cause a concentration-dependent, barbed-end elongation of microvillus-type parallel actin bundles in transfected epithelial cells [32,34]. Like espin-

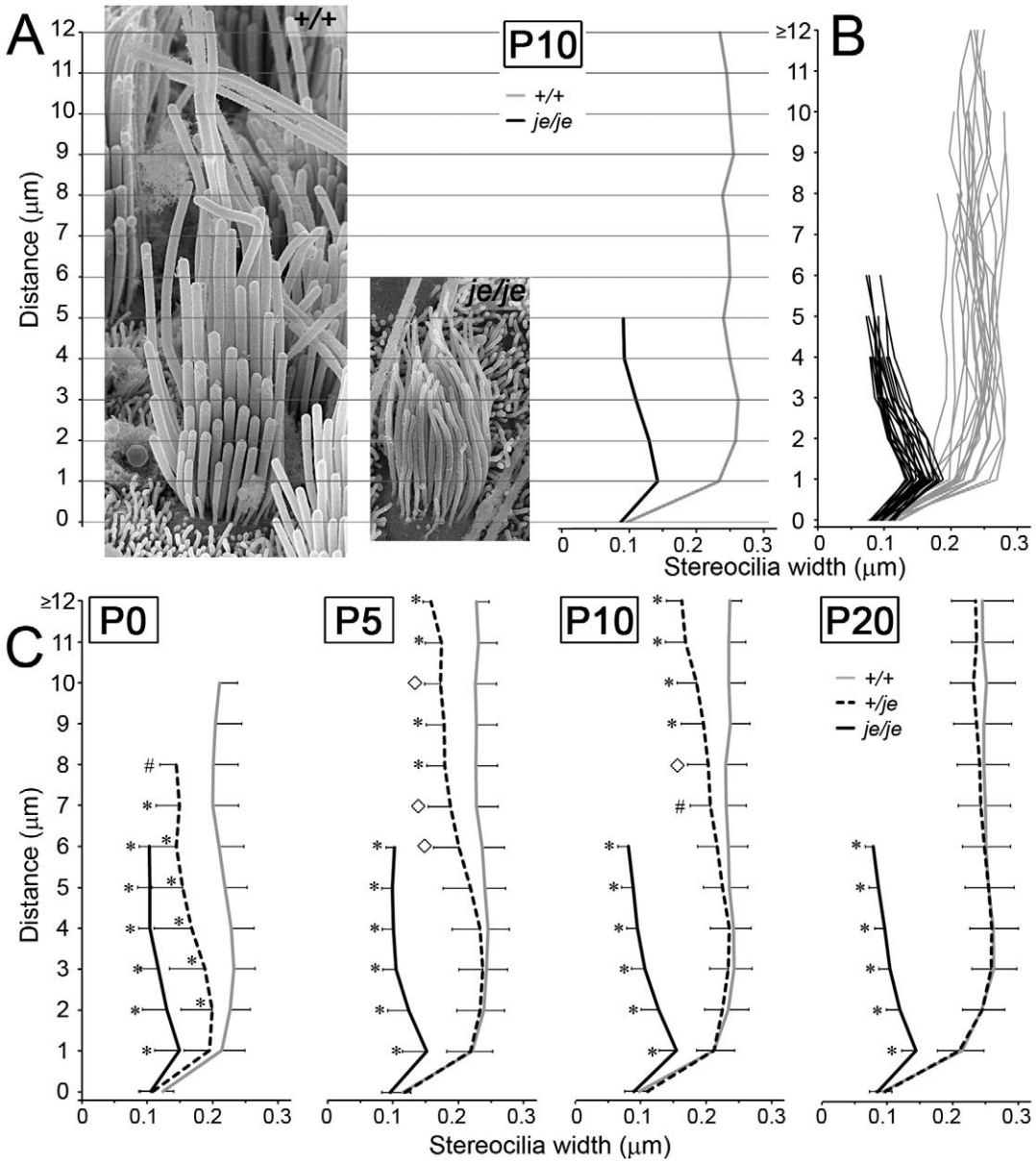

Figure 11. Stereociliary width measurements for extrastriolar vestibular hair cells in postnatal *+/+*, *+/je*, and *je/je* mice. Widths of extrastriolar stereocilia in utricular maculae measured at 1-μm length intervals in mice of the designated genotype and postnatal age are plotted (mean ± SD) as a function of length from the base of the stereocilium. (A) Exemplars of extrastriolar stereocilia in +/+ mice (left) and *je/je* mice (right) at P10. Graph at right shows measurement results for the two stereociliary collections shown in A. (B) Measurements from extrastriolar hair cells in P10 +/+ mice (gray; n = 22 cells) and P10 *je/je* mice (black; n = 23 cells). (C) Combined measurements from mice of each genotype and postnatal age are graphed as mean ± SD. Statistically significant differences from +/+ control are indicated with symbols: *, $p<0.001$; #, $p<0.01$; ◇, $p<0.05$. Note that stereocilia in *je/je* mice are significantly thinner than those in +/+ mice at all time points. However, their distal segment appears thinner than their proximal segment, which indicates a gradual proximal-distal tapering. Stereocilia in *+/je* mice are of intermediate width and differ significantly from those in +/+ mice at lengths of 2 μm and beyond at P0. From P0 through P20, the stereocilia in *+/je* mice gradually become more similar to those in +/+ mice and appear to widen in a proximal-distal direction.
doi:10.1371/journal.pgen.1002032.g011

mediated actin filament bundling [28], the 116-amino acid espin carboxy-terminal actin-bundling module is necessary and sufficient for this barbed-end elongation activity, and putative F-actin-binding sites located at either end of the module are required [32]. Thus, one possibility is that wild-type levels of espin cross-links are needed both to cause the barbed-end elongation of shorter actin filaments situated at the periphery of the parallel actin bundle and to attach the newly elongated filament segments to the bundle. In addition to these activities that emphasize the role of the espin actin-bundling module, espins can bind monomeric actin via their WH2 domain [27,32,57] and can elicit WH2 domain-dependent parallel actin bundle formation when targeted to specific locations – centrosomes [57], nucleoli [57] or filopodial tips [23] – in transfected cells. Thus, it is possible that wild-type espin levels are also needed to deliver polymerizable actin monomer into the stereocilium and to sustain the actin polymerization reactions needed to increase the number and length of actin filaments at the periphery of the parallel actin bundle.

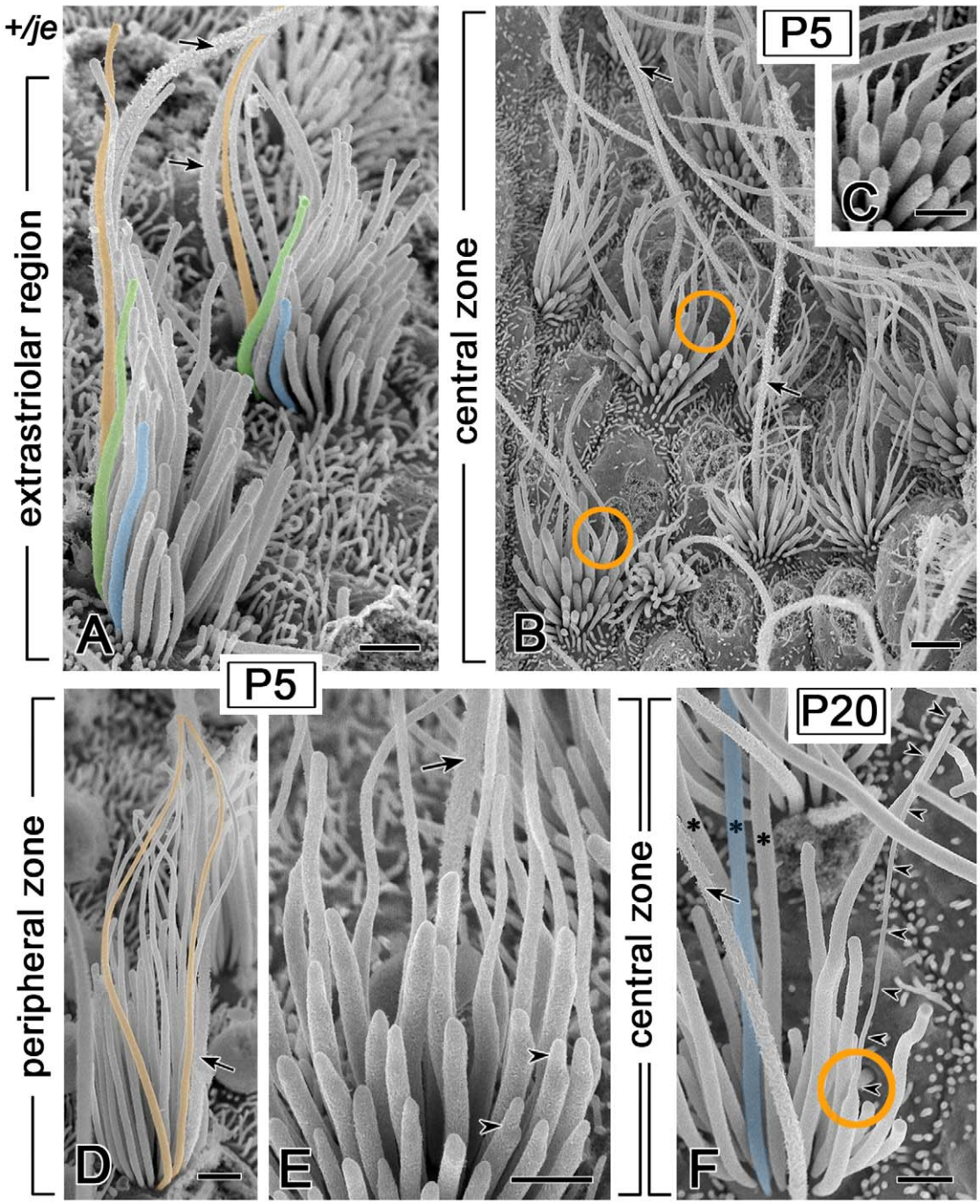

Figure 12. Transient tapering of stereocilia on the vestibular hair cells of *+/je* mice. Kinocilium, arrow. (A) Extrastriolar stereocilia in the utricular macula of a P5 *+/je* mouse illustrating the proximal-distal tapering quantified in Figure 11C. Well-resolved examples of stereocilia showing the tapering are shaded orange or green, whereas shorter stereocilia showing the more normal cylindrical shape are shaded blue. (B,C) Many hair cells in the central zone of the cristae ampullares in early postnatal *+/je* mice have stereocilia with extremely thin distal segments, reminiscent of a candle with a wick (orange circles in B). This specimen is from a P5 *+/je* mouse. (C) shows examples of this abrupt and extreme proximal-distal tapering at higher magnification. (D) In the peripheral zone of the cristae in early postnatal *+/je* mice, many stereocilia show gradual proximal-distal tapering. Two examples of tapered stereocilia in this specimen from a P5 *+/je* mouse are shaded orange. (E) In the central zone of P5 *+/je* mice, some stereocilia show eccentric protruding tips (arrowheads), which are suggestive of intermediates in the process of elongation. (F) By P20, most stereocilia in the central zone of *+/je* mice have increased in diameter, so that the width of the distal portion matches that of the proximal portion (asterisks and example shaded blue). Only an occasional stereocilium (orange circle and arrowheads) retains an extremely thin distal segment at P20. Scale bars, 1 μm (A,C–F) or 2 μm (B).
doi:10.1371/journal.pgen.1002032.g012

A slowing of stereociliary morphogenesis in *+/je* mice might also account for the eccentric protruding distal tips of stereocilia we observed in the central zone of cristae ampullares at P5. These structures, which may represent pioneering elongation intermediates of reduced diameter, are a potential source of the abruptly tapered distal segments of stereocilia ("wicks") we observed as

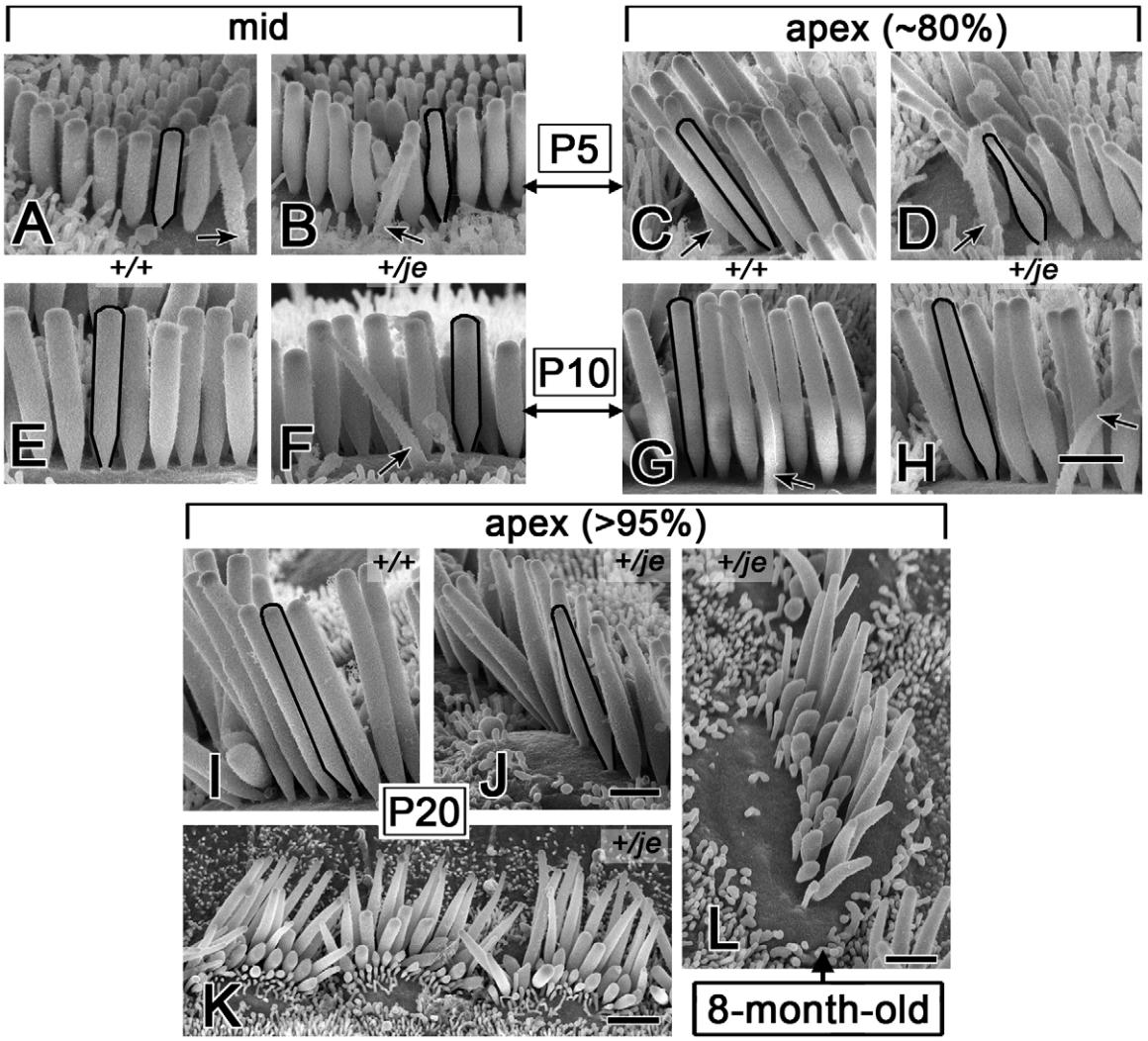

Figure 13. Tapering of stereocilia on the inner hair cells of *+/je* mice. (A–H) Stereocilia on inner hair cells in the middle and apical cochlear regions of *+/je* mice show obvious tapering along their proximal-distal axis (B,D). This tapered segment becomes mostly (F) or partly (H) filled in by P10. The tapering is not observed for the stereocilia of +/+ mice (A,E,C,G). Black outlines highlight examples (kinocilium, arrow). (I-L) In the extreme apex (>95% from base), proximal-distal tapering of stereocilia is evident in *+/je* mice at P20 (J,K), but not in +/+ control mice (I), and can still be seen at 8 months (L). Scale bars, 1 μm (A-J,L) or 2 μm (K).
doi:10.1371/journal.pgen.1002032.g013

assembly intermediates in the central zone of early postnatal *+/je* mice. Thus, with the slowing brought about by reduced espin levels, the morphogenesis of these long vestibular stereocilia beyond the immature stage (Figure 5A) appears resolvable into two additional phases of elongation, each requiring an increase in stereociliary diameter: a phase A that produces stereocilia of relatively similar intermediate length and a phase B involving differential elongation to final length. In the vestibular hair cells of *je/je* mice, stereociliary morphogenesis appears to stall when the increase in diameter associated with phase A does not proceed to completion. Unlike the situation in *je/je* mice, stereocilia in *+/je* mice can largely recover from having reduced espin levels. In fact, we found aged *+/je* mice to be remarkably similar to +/+ mice in stereociliary morphology, hair cell abundance and auditory brainstem response thresholds. Thus, we conclude that the jerker mutation is indeed recessive and that the stereociliary degeneration, extensive hair cell loss and deafness observed previously by Sjöström and Anniko [45–48] in aged jerker heterozygotes of an uncharacterized genetic background are attributable to another influence, e.g., a genetic modifier, age-related hearing loss or disease.

Length defects and differential elongation

Although multiple studies have suggested a connection between espins and the elongation of stereocilia [23,32–35], our results indicate that the relationship between espins and stereociliary length is complicated. It is true that, in general, we found the stereocilia of *je/je* mice to be significantly shorter than their counterparts in +/+ mice. However, we determined that this seemingly generic response to a lack of espins actually reflects a complicated mixture of defects in stereociliary morphogenesis, affecting width and length, together with defects in stereociliary stability, which vary according to inner ear region. For example, the early-stage graded elongation of stereociliary precursors appears remarkably similar in the presence and absence of espins. Cochlear stereocilia are shorter in *je/je* mice primarily because they subsequently shorten and disappear. Our examination of extrastriolar hair cells in the utricular macula suggests that, for

long vestibular stereocilia, it is elongation phase B, involving the final differential elongation, that is markedly attenuated in *je/je* mice. Although espins could contribute directly to this differential elongation through the parallel actin bundle elongation activity mentioned above [32], it is also possible that they contribute in a more indirect manner. For example, a certain threshold in the number of espin cross-links, in actin filament twist or in parallel actin bundle diameter might need to be attained before additional stereocilium elongation can proceed via mechanisms involving other proteins. Construction of a taller stereocilium might simply require a broader base with suitable cross-links. Importantly, stereocilia in the vestibular system of *je/je* mice showed pronounced elongation beyond the precursor stage, e.g., up to lengths of ~6 μm in utricular maculae and ~8 μm in cristae. Thus, clearly substantial stereociliary elongation can take place in the absence of espins.

Degeneration and stabilization

Superimposed on an inability of stereocilia to widen and elongate fully, we observed major defects in stereocilium stability in *je/je* mice. This was especially noticeable in the cochlea, where stereocilia rapidly shortened and disappeared, often so fast as to obscure defects in morphogenesis. A qualitatively different and slower form of stereociliary collapse and resorption was evident in the striolar/central regions of the vestibular system in *je/je* mice. Thus, espins are required to avoid these types of degenerative change, which are suggestive of mechanical weakness, fragmentation and/or depolymerization of the stereocilium's parallel actin bundle scaffold. A likely possibility is that the espins' high-affinity, Ca^{2+}-resistant cross-links are needed to stabilize the parallel actin bundle against depolymerization, fragmentation and mechanical insult. Actin-bundling proteins are known to retard actin depolymerization in vitro [58,59], and an espin-mediated increase in the number of actin filaments in the parallel actin bundle would be expected to make the bundle more sturdy [60]. In a related way, the presence or absence of espin cross-links could determine why some parallel actin bundle-containing projections (stereocilia) are spared while others (microvilli) are cleared from the apical surface of the hair cell during stereociliary morphogenesis in +/+ mice. The occasional loss of a short-row stereocilium from outer hair cells that we observed in +/*je* mice could reflect a similar, yet localized parallel actin bundle disassembly process initiated when espin levels drop below a critical threshold. Higher levels of immunolabeling for espins have been detected at suspected sites of stereociliary damage [61], raising the intriguing possibility that espins may also play important roles in parallel actin bundle repair. Thus, it is conceivable that the various types of stereociliary degeneration we observed in *je/je* mice are extreme manifestations of faulty parallel actin bundle repair. Remarkably, stereocilia in the extrastriolar/peripheral regions of the *je/je* mouse vestibular system, although abnormally thin and short, resisted shortening and collapse for much longer periods, even though we showed that these stereocilia normally contain espins. Since the striolar/central and extrastriolar/peripheral regions contain similar numbers of type I and type II hair cells [55,62], we conclude that the pattern of stereociliary degeneration in the vestibular system of *je/je* mice varies primarily according to region instead of vestibular hair cell type. These differences could be tied to known regional differences in parameters such as hair cell birth date [63], afferent response characteristics [64], hair cell physiology [65] or interstereociliary links [66], but could also reflect regional differences in stereociliary actin dynamics or actin-cytoskeletal proteins.

Espins versus other actin-bundling proteins

Parallel actin bundles in cells typically contain multiple classes of actin-bundling protein [3]. Accordingly, espins are not the only actin-bundling proteins in hair cell stereocilia. The other actin-bundling proteins believed to be present include plastin 1 (I-fimbrin), plastin 3 (T-fimbrin), fascin-2 and TRIOBP, and all except fascin-2 are believed to be present in hair cells in early postnatal development [15–17,35,67]. Given the multiplicity of actin-bundling proteins, it is truly remarkable that these other actin-bundling proteins and the espin-like protein, which has also been detected in stereocilia [17], are insufficient to compensate for the lack of espins in *je/je* mice. Like fimbrins/plastins and fascin, espins are relatively small monomeric globular proteins that preferentially cross-link actin filaments in parallel fashion [30,31,68,69]. The fact that espins show no obvious sequence homology with fimbrins/plastins and fascins raises the possibility that they supply cross-links of a qualitatively different nature. Accordingly, espin cross-links are much more potent than those of fascin at over-twisting the actin filaments in parallel actin bundles [31]. This over-twisting, which likely reflects a high degree of conformational rigidity in the espins, is predicted to allow for an optimum number of interfilament cross-links to form and could lead to enhanced stability for the parallel actin bundle [31]. Actin filament bundling and the cooperative effect on actin filament twist are both realized even at relatively low espin stoichiometry (espin-actin ratio, ~1/50) [29,31]. This may be important because, despite the intense espin antibody labeling we observed along vestibular stereocilia (Figure 1C and 1E), one group recently reported that they recovered espin tryptic peptides at lower yield than those from other actin-bundling proteins in ripped-off preparations of chicken and rat vestibular hair cell stereocilia [17]. Irrespective of their actual stoichiometry, however, we conclude that espins fulfill indispensable and relatively early roles in the multistep assembly of the stereociliary parallel actin bundle. A precedent for multistep parallel actin bundle assembly can be seen in the developing neurosensory bristles of Drosophila, which form through the sequential actions of a putative espin ortholog, forked, followed by a fascin ortholog, singed [70]. Shin et al. [17] recently showed that fascin-2 appeared in stereociliary parallel actin bundles relatively late during the differential elongation of stereocilia and tended to concentrate near the distal end of the longest stereocilia. Thus, the sequential actions of espin and fascin-2 in hair cell stereocilia may be orthologous to the sequential actions of forked and singed in Drosophila bristle parallel actin bundles. A lack of espins may not only impede later-acting actin-bundling proteins, but might also irretrievably impair the parallel actin bundle substrate on which the other proteins involved in length regulation and mechanoelectrical signal transduction depend.

Materials and Methods

Ethics statement

This study was carried out on mice in strict accordance with the recommendations in the Guide for the Care and Use of Laboratory Animals of the National Institutes of Health. The protocol was approved by the Northwestern University Animal Care and Use Committee (Protocols 2004-0427, 2007-0427 and 2008-1321). Perfusion fixation and measurements of auditory brainstem response were performed under sodium pentobarbital anesthesia. Organ removal for western blotting was performed following euthanasia under CO2 gas-induced narcosis by decapitation with a rodent guillotine. All efforts were made to minimize animal suffering.

Animals

Inbred CBA/CaJ mice (stock number 000654) and jerker mice of the standard commercially available strain (JE/LeJ; stock number 000259) were purchased from the Jackson Laboratory and bred and housed in the barrier-level mouse vivarium in the Center for Comparative Medicine at Northwestern University Feinberg School of Medicine. Homozygous jerker males were bred with heterozygous jerker or wild-type females. Homozygous animals older than P10 could be identified by their distinctive shaker-waltzer behavior. Genotypes were confirmed by DNA sequence analysis of PCR products obtained from tail genomic DNA [14]. We produced the congenic jerker mouse line used in this study (CBA/CaJ.JE/LeJ-*Espn*^{je}) by repeated backcrossing into the CBA/CaJ inbred strain for 13–15 generations, according to the following scheme: male jerker homozygotes of generation n were mated with wild-type CBA/CaJ females, and the resulting heterozygous progeny from two different breeder pairs were mated to produce male jerker homozygotes of generation n+1. Approximately every 3 generations, the wild-type CBA/CaJ female breeder stock was refreshed with mice newly purchased from the Jackson Laboratory. Wild-type mice of the JE/LeJ strain were produced by mating heterozygotes and identified by genotyping.

Immunohistochemistry

Mice were anesthetized by intraperitoneal injection with sodium pentobarbital (60 mg/kg) and briefly perfused through the ascending aorta with 0.9% (w/v) NaCl followed by fixative solution: 4% (w/v) formaldehyde (freshly prepared from paraformaldehyde) in 0.1 M sodium phosphate buffer, pH 7.4. The inner ear was removed by dissection. A small hole was made at the top of the cochlea with the tip of a fine forceps, and the semicircular canals were broken open. Through these openings the inner ear was gently flushed with ~0.3 ml of 2% (w/v) paraformaldehyde in 0.1 M sodium phosphate buffer, pH 7.4, and then postfixed for an additional 1 h. Utricular maculae were dissected away from bony labyrinths. To carefully expose the epithelium, the overlying membranous labyrinth was removed, and the otoconial membrane was gently removed using a single strand from a brush. Specimens were treated with 3% (v/v) normal goat serum, 1% (w/v) bovine serum albumin, 0.2% (v/v) Triton X-100 in TBS (100 mM Tris, 150 mM NaCl, pH 7.4), and incubated overnight with affinity purified rabbit polyclonal espin antibody at a concentration of 1 µg/ml. The espin antibody, which we raised against purified recombinant rat espin 2B and affinity purified on columns of rat espin 2B-Sepharose 4B, is known to react with all espin isoforms, including epitopes that are amino-terminal to site of the frameshift mutation in jerker espins [27,51]. The bound antibody was detected by Alexa594-goat anti-rabbit IgG (Invitrogen). F-actin was visualized using Alexa488-phalloidin (Invitrogen). Specimens were mounted with Vectashield (Vector Laboratories) and examined using the Nikon PCM2000 system confocal microscope and Simple PCI Program.

Dissected cerebella were cryoprotected in 30% (w/v) sucrose dissolved in phosphate-buffered saline. Frozen sections, 30 µm thick, were cut in the sagittal plane on a freezing-stage sliding microtome. For bright-field microscopy, sections were processed for immunohistochemistry according to an avidin-biotin amplification protocol. Briefly, the endogenous peroxidase activity was blocked with 0.3% (v/v) H_2O_2 and 10% (v/v) methanol in TBS. Sections were treated with 3% (v/v) normal goat serum, 1% (w/v) bovine serum albumin, 0.2% (v/v) Triton X-100 in TBS and then incubated with either mouse anti-calbindin monoclonal antibody (1:5,000; Sigma) or affinity purified rabbit polyclonal espin antibody (see above). Bound antibody was detected using biotinylated donkey anti-mouse or anti-rabbit IgG (GE Healthcare), the ABC Elite kit (Vector Laboratories) and diaminobenzidine (Sigma). Images were captured with the Spot RT CCD video camera (Diagnostics Instruments) mounted on the Nikon Eclipse 800 microscope using the Spot RT Software 3.5.8. Whole-mount images of eyes were captured with the Nikon digital DN100 camera mounted on the Olympus SZH10 stereomicroscope. All images were stored and processed in Adobe Photoshop CS2. Brightness and contrast were adjusted.

Western blotting

Mice (~6 months old) were euthanized by decapitation while under CO_2 gas-induced narcosis. Testes and kidneys were removed by dissection, weighed and homogenized in 9 (kidney) or 18 (testis) volumes (ml/g) of ice-cold 0.25 M sucrose, 3 mM imidazole-HCl, pH 7.4, containing 2 mM phenylmethylsulfonyl fluoride and 1% (v/v) Protease Inhibitor Cocktail (Sigma P 8849) using 8 up-and-down strokes of a motor-driven 10-ml Teflon-glass Potter-Elvehjem homogenizer spinning at 3000 rpm. SDS gel buffer concentrate containing dithiothreitol was added, and the samples were heated at 95-100°C for 3 min with intermittent agitation on a vortex mixer. Gel samples derived from 1.8 mg (testis) or 3.6 mg (kidney) of wet tissue mass were resolved in SDS gels and transferred to nitrocellulose membrane. The blots were labeled with affinity purified rabbit polyclonal espin antibody (see above) at a concentration of 0.1 µg/ml using the ECL system (GE Healthcare). Apparent molecular mass was estimated using the BenchMark Prestained Protein Ladder (Invitrogen).

Scanning electron microcopy

Mice of the designated age and of either sex were anesthetized by intraperitoneal injection with sodium pentobarbital (60 mg/kg) and briefly perfused through the ascending aorta with 0.9% (w/v) NaCl followed by 5-20 ml of fixative solution: 2.5% glutaraldehyde and 2 mM $CaCl_2$ in 0.1 M sodium cacodylate buffer, pH 7.4. The inner ear was removed by dissection. A small hole was made at the top of the cochlea with the tip of a fine forceps, and the semicircular canals were broken open. Through these openings the inner ear was gently flushed with ~0.3 ml of 2.5% glutaraldehyde fixative solution and then postfixed overnight at 4°C. The membranous labyrinth, containing the cochlea and vestibular end organs, was removed by dissection. Cochlear specimens were prepared by removing the stria vascularis, Reissner's membrane and tectorial membrane. The cochlear spiral was cut into basal, middle and apical segments for processing. The utricular maculae and two adjacent, horizontal and anterior, cristae ampullares were also removed by dissection. The otolithic membrane was gently removed from the macular surface using a single strand from a brush. Specimens were processed using an osmium-thiocarbohydrazide method adapted from Hunter-Duvar [71], which included three 1-h incubations with 1% (w/v) OsO4, with 20-min incubations with saturated thiocarbohydrazide inserted after the first and second OsO_4 treatments. The specimens were then dehydrated using a graded series of ethanol solutions and critical-point dried using liquid CO_2 as the transitional fluid. Uncoated specimens were mounted on a Hitachi specimen stub using silver electroconductive paint and viewed using a Hitachi S-4800 field emission scanning electron microscope operated at 5 kV.

Quantification

Stereociliary dimensions were measured using NIH ImageJ (Wayne Rasband, National Institutes of Health, Bethesda, MD;

http://rsb.info.nih.gov/ij/), and analyzed using Instat 3.0 (GraphPad Software). To minimize foreshortening, specimens were rotated and tilted in the scanning electron microscope so that, for the purposes of measurement, the stereocilia under examination were approximately perpendicular to the direction of view. The length and width of cochlear hair cell stereocilia were measured at P0 (n = 3 mice of each genotype) and P5 (n = 2 mice of each genotype). For each mouse, images of 10 outer and 10 inner hair cells were collected at 20,000X magnification from each of three different cochlear locations: base (~20% from base), mid (~50% from base) and apex (~80% from base). We measured the lengths of the 4 tallest stereocilia and the widths of 5 randomly selected stereocilia on each cochlear hair cell. The perpendicular alignment of stereocilia was difficult to accomplish for cochlear specimens from *je/je* mice, because these stereocilia were often bent in different directions (e.g., Figure 8G). We measured the lengths of the 4 tallest stereocilia on each hair cell, regardless of their location in the collection. In +/+ mice, the tallest stereocilia were located in the tallest row, near the kinocilium, whereas in *je/je* mice the tallest stereocilia could be found at other locations in the collection (e.g., Figure 8H). Widths were measured at 2 different positions, at the midpoint and near the top, and then averaged. The number of total surface projections (stereocilia and microvillus-like structures) on 10 outer hair cells from each row (30 outer hair cells total) at each of the three cochlear locations were counted at P5 and P10 for mice of all three genotypes. Likewise, the numbers of missing stereocilia on outer hair cells, as evidenced by a characteristic gap in the shortest row of stereocilia (Figure 4D and 4E), were counted for +/+ and +/*je* mice at P10.

The width of stereocilia on extrastriolar hair cells was measured at 1-μm intervals along the length. The analysis included 3 or 4 mice of each of the three genotypes at P0, P5, P10 and P20, 2 *je/je* mice at P40 and 1 *je/je* mouse each at P60 and P90. To avoid immature hair cells (e.g., Figure 5A and 5B), only hair cells with stereocilia of lengths >7 μm (+/+ or +/*je*) or >3 μm (*je/je*) were included. Images of the stereociliary collection (n = 20–28 hair cells for each genotype and each time point) were transferred to Adobe Photoshop, where a grid of lines (spaced at 1-μm intervals) was placed over the image (Figure 11A). Widths were measured for clearly resolved stereocilia that crossed a line or, in the case of the distal tip, ended close to a line. In addition, we measured widths at the extreme base, where the stereocilia emerged from the apical surface of the hair cell. The width measurements at each distance were averaged for individual hair cells (see graph in Figure 11A). These data were combined (Figure 11B) to calculate mean ± SD for each genotype and postnatal age (Figure 11C). In most instances, we obtained large numbers of measurements (>100), which did not show a Gaussian distribution. Therefore, such measurements were analyzed using the nonparametric Kruskal-Wallis test followed by Dunn's multiple comparisons test. In two instances, sample sizes were, by necessity, considerably smaller and showed a Gaussian distribution: width measurements at 11 and 12 μm from the base of extrastriolar stereocilia (Figure 11C). These measurements were analyzed by one-way analysis of variance followed by the Bonferroni multiple comparisons test. The average height of the collection of stereocilia on the extrastriolar hair cells of *je/je* mice (Figure 5E) was estimated from measurements of 100 hair cells at each postnatal age.

Auditory brainstem response

Mice were anesthetized by intraperitoneal injection with sodium pentobarbital (initial, 80 mg/kg; maintenance, 17 mg/kg). Auditory brainstem responses were obtained by subtracting ipsilateral mastoid potentials from vertex potentials measured relative to a ground electrode placed in the neck. The electrodes were connected to a differential amplifier (ISO-80, World Precision Instruments) with a high input-impedance ($>10^{12}$ Ω) set to 80 dB. Further filtering of the signal (300–3000 Hz) was obtained through an IP90 filter (Frequency Devices). The sampling rate was 200 kHz, and responses to 100 stimulus presentations were averaged. Auditory brainstem response thresholds were defined as sound levels required for a visible response to acoustic stimuli. The noise floor in an average recording was typically 1 μV. In particular, the appearance of wave II was monitored. Voltage commands for acoustical stimuli were generated using a computer KPCI 3110 I/O board (Keithley Instruments, Inc.) inserted into a personal computer and were used to drive a DT 770Pro headphone (Beyerdynamic). For acoustically evoked auditory brainstem responses, tone bursts (12 ms duration, 1 ms rise/fall) with different carrier frequencies were presented at a rate of 4 Hz. The sound pressure was measured with a real head coupler [72]. Means and standard errors were calculated for the electrophysiological thresholds. Measurements were analyzed by one-way analysis of variance followed by the Tukey-Kramer multiple comparisons test.

Supporting Information

Figure S1 Differences between CBA/CaJ and JE/LeJ mice in cerebellum and eye. (A-D) Near-midline saggital cryosections through the cerebella of adult wild-type (+/+) or homozygous jerker (*je/je*) mice with the CBA/CaJ or JE/LeJ genetic background immunoperoxidase-labeled with antibody to espin (A) or calbindin (B-D) to highlight Purkinje cells and their dendritic trees in the molecular layer of the cerebellum. A simplified pattern of cerebellar lobulation is detected in JE/LeJ mice (C,D) compared to CBA/CaJ mice (A,B). Numeric assignments for the lobules are shown for the CBA/CaJ specimen in panel A. Scale bar, 200 μm. (E) Whole mounts of eyeballs isolated from perfusion-fixed mice with the CBA/CaJ or JE/LeJ genetic background. Small misshapen eyeballs with constricted pupils are commonly detected in wild-type mice and homozygous jerker mice with the JE/LeJ genetic background, but not in wild-type mice and homozygous jerker mice with the CBA/CaJ genetic background. The specimens shown are from homozygous jerker mice. (F) Whole mounts of eye lens isolated from perfusion-fixed mice with the CBA/CaJ or JE/LeJ genetic background. A small lens size and cloudy appearance are commonly detected in wild-type mice and homozygous jerker mice with the JE/LeJ genetic background, but not in wild-type mice and homozygous jerker mice with the CBA/CaJ genetic background. The specimens shown are from homozygous jerker mice.
(TIF)

Figure S2 Relatively normal appearance of hair cells in P0 *je/je* mice and region-specific loss at P20. (A) View of the cochlea from a P0 *je/je* mouse showing how the customary three row of outer hair cells (OHC) and one row of inner hair cells (IHC) are easy to distinguish from the surrounding supporting cells. Note the graded elongation of stereociliary precursors at the kinocilial pole of the cell and the preferential alignment of this pole toward the abneural edge of the epithelium (top of figure). (B,C) At P20, hair cell loss in *je/je* mice is greater in the middle region of the cochlea (C) than in the apical region (B). Examples of positions in the epithelium that are missing outer hair cells (OHC) and grown over by presumptive supporting cells bearing a dense collection of short microvilli are indicated with arrows. IHC, inner hair cells. Scale bars, 10 μm.
(TIF)

Figure S3 Striolar hair cells, bent peripheral zone *je/je* stereocilia and degeneration of extrastriolar stereocilia after P40. Kinocilium,

black arrow. (A-C) Striolar region of utricular maculae. Note the increases in stereociliary width and length observed between P0 and P10 in +/+ mice (A,C) and the abnormally thin and short stereocilia present in *je/je* mice at P0 (B). (D-F) Peripheral zone of cristae ampullares in P5 (D) or P20 (E,F) *je/je* mice showing stereocilia with proximal-distal tapering, an elbow-like bend in their proximal segment (arrowheads), or with an extremely thin distal process in close association with the kinocilium (three white arrows in D). (G-J) Beyond P40, stereocilia on extrastriolar hair cells in utricular maculae gradually shorten and become thinner. Measurements of width versus length, similar to those in Figure 11C, are shown in J. Illustrative images are shown in G-I. Scale bars, 2 μm (A,B) or 1 μm (C-I).
(TIF)

References

1. Vollrath MA, Kwan KY, Corey DP (2007) The micromachinery of mechanotransduction in hair cells. Annu Rev Neurosci 30: 339–365.
2. Schwander M, Kachar B, Müller U (2010) The cell biology of hearing. J Cell Biol 190: 9–20.
3. Bartles JR (2000) Parallel actin bundles and their multiple actin-bundling proteins. Curr Opin Cell Biol 12: 72–78.
4. Tilney LG, Tilney MS, DeRosier DJ (1992) Actin filaments, stereocilia and hair cells: how cells count and measure. Annu Rev Cell Biol 8: 257–274.
5. Frolenkov GI, Belyantseva IA, Friedman TB, Griffith AJ (2004) Genetic insights into the morphogenesis of inner ear hair cells. Nat Rev Genet 5: 489–498.
6. Tilney LG, DeRosier DJ (1986) Actin filaments, stereocilia, and hair cells of the bird cochlea. IV. How the actin filaments become organized in developing stereocilia and in the cuticular plate. Dev Biol 116: 119–129.
7. Tilney LG, Saunders JC (1983) Actin filaments, stereocilia, and hair cells of the bird cochlea. I. Length, number, width, and distribution of stereocilia of each hair cell are related to the position of the hair cell on the cochlea. J Cell Biol 96: 807–821.
8. Tilney LG, Tilney MS, Cotanche DA (1988) Actin filaments, stereocilia, and hair cells of the bird cochlea. V. How the staircase pattern of stereociliary lengths is generated. J Cell Biol 106: 355–365.
9. Kaltenbach JA, Falzarano PR, Simpson TH (1994) Postnatal development of the hamster cochlea: II. Growth and differentiation of stereocilia bundles. J Comp Neurol 350: 197–198.
10. Li A, Xue J, Peterson EH (2008) Architecture of the mouse utricle: macular organization and hair bundle heights. J Neurophysiol 99: 718–733.
11. Dror AA, Avraham KB (2009) Hearing loss: mechanisms revealed by genetics and cell biology. Annu Rev Genet 43: 411–437.
12. Petit C, Richardson GP (2009) Linking genes underlying deafness to hair-bundle development and function. Nat Neurosci 12: 703–710.
13. Tilney MS, Tilney LG, Stephens RE, Merte C, Drenckhahn D, et al. (1989) Preliminary characterization of the stereocilia and cuticular plate of hair cells in the chick cochlea. J Cell Biol 109: 1711–1723.
14. Zheng L, Sekerková G, Vranich K, Tilney LG, Mugnaini E, et al. (2000) The deaf jerker mouse has a mutation in the gene encoding the espin actin-bundling proteins of hair cell stereocilia and lacks espins. Cell 102: 377–385.
15. Daudet N, Lebart M-C (2002) Transient expression of the T-isoform of plastins/fimbrin in the stereocilia of developing auditory hair cells. Cell Motil Cytoskeleton 53: 326–336.
16. Kitajiri S, Sakamoto T, Belyantseva IA, Goodyear RJ, Stepanyan R, et al. (2010) Actin-bundling protein TRIOBP forms resilient rootlets of hair cell stereocilia essential for hearing. Cell 141: 786–798.
17. Shin JB, Longo-Guess CM, Gagnon LH, Saylor KW, Dumont RA, et al. (2010) The R109H variant of fascin-2, a developmentally regulated actin crosslinker in hair-cell stereocilia, underlies early-onset hearing loss of DBA/2J mice. J Neurosci 30: 9683–9694.
18. Peng AW, Belyantseva IA, Hsu PD, Friedman TB, Heller S (2009) Twinfilin 2 regulates actin filament lengths in cochlear stereocilia. J Neurosci 29: 15083–15088.
19. Rzadzinska AK, Nevalainen NK, Prosser HM, Lappalainen P, Steel KP (2009) Myosin VIIA interacts with twinfilin-2 at the tips of mechanosensory stereocilia in the inner ear. PLoS ONE 4: e7097. doi:10.1371/journal.pone.0007097.
20. Mburu P, Romero HR, Hilton H, Parker A, Townsend S, et al. (2010) Gelsolin plays a role in the actin polymerization complex of hair cell stereocilia. PLoS ONE 5: e11627. doi:10.1371/journal.pone.0011627.
21. Belyantseva IA, Boger ET, Naz S, Frolenkov GI, Sellers JR, et al. (2005) Myosin-XVa is required for tip localization of whirlin and differential elongation of hair-cell stereocilia. Nat Cell Biol 7: 148–156.
22. Delprat B, Michel V, Goodyear R, Yamasaki Y, Michalski N, et al. (2005) Myosin XVa and whirlin, two deafness gene products required for hair bundle growth, are located at stereocilia tips and interact directly. Hum Mol Genet 14: 401–410.
23. Salles FT, Merritt RC, Jr., Manor U, Doherty GW, Sousa AD, et al. (2009) Myosin IIIa boosts elongation of stereocilia by transporting espin 1 to the plus ends of actin filaments. Nat Cell Biol 11: 443–450.
24. Sekerková G, Zheng L, Loomis PA, Mugnaini E, Bartles JR (2006) Espins and the actin cytoskeleton of hair cell stereocilia and sensory cell microvilli. Cell Mol Life Sci 63: 2329–241.
25. Bartles JR, Wierda A, Zheng L (1996) Identification and characterization of espin, an actin-binding protein localized to the F-actin-rich junctional plaque of Sertoli cell ectoplasmic specializations. J Cell Sci 110: 1229–1239.
26. Sekerková G, Loomis PA, Changyaleket B, Zheng L, Eytan R, et al. (2003) Novel espin actin-bundling proteins are localized to Purkinje cell dendritic spines and bind the Src homology 3 adapter protein insulin receptor substrate p53. J Neurosci 23: 1310–1319.
27. Sekerková G, Zheng L, Loomis PA, Changyaleket B, Whitlon DS, et al. (2004) Espins are multifunctional actin cytoskeletal regulatory proteins in the microvilli of chemosensory and mechanosensory cells. J Neurosci 24: 5445–5456.
28. Bartles JR, Zheng L, Li A, Wierda A, Chen B (1998) Small espin: a third actin-bundling protein and potential forked protein ortholog in brush border microvilli. J Cell Biol 143: 107–119.
29. Chen B, Li A, Wang D, Wang M, Zheng L, et al. (1999) Espin contains an additional actin-binding site in its N terminus and is a major actin-bundling protein of the Sertoli cell-spermatid ectoplasmic specialization junctional plaque. Mol Biol Cell 10: 4327–4339.
30. Purdy KR, Bartles JR, Wong GC (2007) Structural polymorphism of the actin-espin system: a prototypical system of filaments and linkers in stereocilia. Phys Rev Lett 98: 08105.
31. Shin H, Purdy Drew KR, Bartles JR, Wong GCL, Grason GM (2010) Cooperativity and frustration in protein-mediated parallel actin bundles. Phys Rev Lett 103: 238102.
32. Loomis PA, Zheng L, Sekerková G, Changyaleket B, Mugnaini E, et al. (2003) Espin cross-links cause the elongation of microvillus-type parallel actin bundles in vivo. J Cell Biol 163: 1045–1055.
33. Rzadzinska A, Schneider M, Noben-Trauth K, Bartles JR, Kachar B (2005) Balanced levels of espin are critical for stereociliary growth and length maintenance. Cell Motil Cytoskeleton 62: 157–165.
34. Zheng L, Zheng J, Whitlon DS, Garcia-Añoveros J, Bartles JR (2010) Targeting of the hair cell proteins cadherin 23, harmonin, myosin XVa, espin and prestin in an epithelial cell model. J Neurosci 30: 7187–7201.
35. Sekerková G, Zheng L, Mugnaini E, Bartles JR (2006) Differential expression of espin isoforms during epithelial morphogenesis, stereociliogenesis and postnatal maturation in the developing inner ear. Dev Biol 291: 83–95.
36. Furness DN, Mahendrasingam S, Ohashi M, Fettiplace R, Hackney CM (2008) The dimensions and composition of stereociliary rootlets in mammalian cochlear hair cells: comparison between high- and low-frequency cells and evidence for a connection to the lateral membrane. J Neurosci 28: 6342–6353.
37. Li H, Liu H, Balt S, Mann S, Corrales CE, et al. (2004) Correlation of expression of the actin filament-bundling protein espin with stereociliary bundle formation in the developing inner ear. J Comp Neurol 468: 125–134.
38. Oshima K, Shin K, Diensthuber M, Peng AW, Ricci AJ, et al. (2010) Mechanosensitive hair cell-like cells from embryonic and induced pluripotent stem cells. Cell 141: 704–716.
39. Naz S, Griffith AJ, Riazuddin S, Hampton LL, Battey JF, Jr., et al. (2004) Mutations of *ESPN* cause autosomal recessive deafness and vestibular dysfunction. J Med Genet 41: 591–595.
40. Donaudy F, Zheng L, Ficarella R, Ballana E, Carella M, et al. (2006) Espin gene (*ESPN*) mutations associated with autosomal dominant hearing loss cause defects in microvillar elongation or organization. J Med Genet 43: 157–161.
41. Grüneberg H, Burnett JB, Snell GD (1941) The origin of jerker, a new gene mutation of the house mouse, and linkage studies made with it. Proc Natl Acad Sci USA 27: 562–565.
42. Deol MS (1954) The anomalies of the labyrinth of the mutants varitint-waddler, shaker-2 and jerker in the mouse. J Genet 52: 562–565.

Acknowledgments

We thank Dr. Lili Zheng and Dina Beeler for valuable assistance, Drs. David Furness and Agnieszka Rzadzinska for advice about scanning electron microscopy, Drs. Jaime García-Añoveros and Donna Whitlon for comments on the manuscript, and anonymous reviewers for helpful suggestions.

Author Contributions

Conceived and designed the experiments: GS C-PR JRB. Performed the experiments: GS C-PR JRB. Analyzed the data: GS C-PR JRB. Contributed reagents/materials/analysis tools: GS C-PR JRB. Wrote the paper: GS JRB.

43. Steel KP, Bock GR (1983) Cochlear dysfunction in the jerker mouse. Behav Neurosci 97: 381–391.
44. Jackson T, Thomas J, Green ED, Noben-Trauth K (2002) Genetic and physical maps of jerker (*Espn*^{je}) on mouse chromosome 4. Biochem Biophys Res Commun 296: 1143–1147.
45. Sjöström B, Anniko M (1990) Morphologically specific vestibular hair cell degeneration in the jerker mutant mouse. Eur Arch Otorhinolaryngol 247: 51–55.
46. Sjöström B, Anniko M (1992) Cochlear structure and function in a recessive type of genetically induced inner ear degeneration. ORL J Otorhinolaryngol Relat Spec 54: 220–228.
47. Sjöström B, Anniko M (1992) Genetically induced inner ear degeneration. A structural and functional study. Act Otolaryngol Suppl (Stockh) 493: 141–146.
48. Sjöström B, Anniko M (1990) Variability in genetically induced age-related impairment of auditory brainstem response thresholds. Acta Otolaryngol 109: 353–360.
49. Johnson KR, Zheng QY, Noben-Trauth K (2006) Strain background effects and genetic modifiers of hearing in mice. Brain Res 1091: 79–88.
50. Zheng QY, Johnson KR, Erway LC (1999) Assessment of hearing in 80 inbred strains of mice by ABR threshold analyses. Hear Res 130: 94–107.
51. Sekerková G, Zheng L, Mugnaini E, Bartles JR (2008) Espin actin-cytoskeletal proteins are in rat type I spiral ganglion neurons and include splice-isoforms with a functional nuclear localization signal. J Comp Neurol 509: 661–676.
52. Roth B, Bruns V (1992) Postnatal development of the rat organ of Corti: II. Hair cell receptors and their supporting elements. Anat Embryol (Berl) 185: 571–581.
53. Shnerson A, Willott JF (1980) Ontogeny of the acoustic startle response in C57BL/6J mouse pups. J Comp Physiol Psychol 94: 36–40.
54. Etournay R, Lepelletier L, Boutet de Monvel J, Michel V, Cayet N, et al. (2010) Cochlear outer hair cells undergo an apical circumference remodeling constrained by the hair bundle shape. Development 137: 1373–1383.
55. Desai SS, Zeh C, Lysakowski A (2005) Comparative morphology of rodent vestibular periphery. I. Saccular and utricular maculae. J Neurophysiol 93: 251–266.
56. Lelli A, Asai Y, Forge A, Holt JR, Géléoc GS (2009) Tonotopic gradient in the developmental acquisition of sensory transduction in outer hair cells of the mouse cochlea. J Neurophysiol 101: 2961–2973.
57. Loomis PA, Kelly AE, Zheng L, Changyaleket B, Sekerková G, et al. (2006) Targeted wild-type and jerker espins reveal a novel, WH2-domain-dependent way to actin bundles in cells. J Cell Sci 119: 1655–1665.
58. Zigmond SH, Furukawa R, Fechheimer M (1992) Inhibition of actin filament depolymerization by the Dictyostelium 30,000-D actin-bundling protein. J Cell Biol 119: 559–567.
59. Schmoller KM, Semmrich C, Bausch AR (2011) Slow-down of actin depolymerization by cross-linking molecules. J Struct Biol 173: 350–357.
60. Shin JH, Mahadevan L, So PT, Matsudaira P (2004) Bending stiffness of a crystalline actin bundle. J Mol Biol 337: 255–261.
61. Belyantseva IA, Perrin BJ, Sonnemann KJ, Zhu M, Stepanyan R, et al. (2009) Gamma-actin is required for cytoskeletal maintenance but not development. Proc Natl Acad Sci USA 106: 9703–9708.
62. Desai SS, Ali H, Lysakowski A (2005) Comparative morphology of the rodent vestibular periphery. II. Cristae ampullares. J Neurophysiol 93: 267–280.
63. Sans A, Chat M (1982) Analysis of temporal and spatial patterns of rat vestibular hair cell differentiation by tritiated thymidine radioautography. J Comp Neurol 206: 1–8.
64. Goldberg JM, Desmadryl G, Baird RA, Fernández C (1990) The vestibular nerve of the chinchilla. V. Relation between afferent discharge properties and peripheral innervation patterns in the utricular macula. J Neurophysiol 63: 791–804.
65. Wooltorton JRA, Gaboyard S, Hurley KM, Price SD, Garcia JL, et al. (2007) Developmental changes in two voltage-dependent sodium currents in utricular hair cells. J Neurophysiol 97: 1684–1704.
66. Goodyear R, Richardson G (1992) Distribution of the 275 kD hair cell antigen and cell surface specialisations on auditory and vestibular hair bundles in the chicken inner ear. J Comp Neurol 325: 243–256.
67. Zine A, Hafidi A, Romand R (1995) Fimbrin expression in the developing rat cochlea. Hear Res 87: 165–169.
68. Volkmann N, DeRosier D, Matsudaira P, Hanein D (2001) An atomic model of actin filaments cross-linked by fimbrin and its implications for bundle assembly and function. J Cell Biol 153: 947–956.
69. Claessens MM, Semmrich C, Ramos L, Bausch AR (2008) Helical twist controls the thickness of actin bundles. Proc Natl Acad Sci USA 105: 8819–8822.
70. Tilney LG, Connelly PS, Vranich KA, Shaw MK, Guild GM (1998) Why are two different cross-linkers necessary for actin bundle formation in vivo and what does each cross-linker contribute? J Cell Biol 143: 121–133.
71. Hunter-Duvar IM (1978) A technique for preparation of cochlear specimens for assessment with the electron microscope. Acta Otolaryngol 351: 3–23.
72. Pearce M, Richter C-P, Cheatham MA (2001) A reconsideration of sound calibration in the mouse. J Neurosci Methods 106: 57–67.